

A comparative study of the S_1 and U_1 leptoquark effects at IceCube

ILJA DORŠNER ^a, SVJETLANA FAJFER ^{b,c} AND MONALISA PATRA ^b

^a *University of Split, Faculty of Electrical Engineering, Mechanical Engineering and Naval Architecture in Split (FESB), Ruđera Boškovića 32, 21000 Split, Croatia*

^b *Jožef Stefan Institute, Jamova 39, P.O. Box 3000, 1001 Ljubljana, Slovenia*

^c *Department of Physics, University of Ljubljana, Jadranska 19, 1000 Ljubljana, Slovenia*

We study the phenomenology of two leptoquarks, the Standard Model $SU(2)$ singlets S_1 and U_1 , with regard to the latest experimental data from the IceCube Collaboration. We consider a scenario when scalar (vector) leptoquark S_1 (U_1) couples exclusively to the down quark and the neutrinos (charged leptons) of all flavors. The couplings of S_1 (U_1) to the up-type quarks and the charged leptons (neutrinos) are in turn uniquely determined via $SU(2)$ symmetry. We add, in both cases, the leptoquark induced events to the Standard Model ones and perform a χ^2 fit to quantify the overall agreement with the IceCube data. We further analyse whether the inferred allowed parameter space is consistent with the latest LHC data and various low-energy flavor physics measurements. We find that both leptoquarks exhibit the same level of inadequacy in explaining the current IceCube data but for different reasons. Our study offers an up-to-date analysis for these two leptoquarks in view of the latest experimental measurements.

1 Introduction

The observation of high-energy neutrinos at the South Pole situated IceCube detector has ushered in a beginning of extragalactic high-energy neutrino astronomy [1–3]. After six years of data taking, from early 2010 to early 2016, for a total livetime of 2078 days, this 1 km³ detector has observed 80 High Energy Starting Events (HESE) (plus 2 events which could not be reconstructed). This observation is consistent with an isotropic, astrophysical, high-energy, all flavor neutrino flux. The source or sources of most of the observed astrophysical neutrino flux still remains unclear. The IceCube Collaboration has found evidence for neutrino emission from the blazar TXS 0506+056 through the observation of a high-energy astrophysical neutrino flux [4, 5] in 2018. The total neutrino flux from this source is however less than 1% of the total observed astrophysical flux. There have also been other studies by the IceCube Collaboration, with the search optimized for point-like sources, using the neutrino emission with the same flux characteristics as the observed astrophysical muon-neutrino flux [6].

The observation of the HESE events above 100 TeV that is consistent with a flux of high-energy astrophysical neutrinos from outside the galaxy has motivated a large number of studies that explore the IceCube potential to test various New Physics (NP) models. Some of the most explored NP sources are the various leptoquark (LQ) scenarios. The LQs couple a Standard Model (SM) quark to a lepton and emerge in a natural way in many NP proposals such as the Grand Unified Theories based on $SU(5)$, $SO(10)$ [7, 8], supersymmetry with R-parity violation [9], and composite models [10, 11]. There are 12 (10) types of LQ multiplets [12] under the SM gauge group $SU(3) \times SU(2) \times U(1)$ if one assumes presence (absence) of right-handed neutrinos. These multiplets can either be of scalar or vector nature but are, in all instances, triplets under $SU(3)$. The LQ masses as well as the strengths of associated couplings to the SM fermions depend on the ultraviolet completion of the theory from which the LQs presumably descend. These masses and coupling strengths span the parameter space whose viability under the IceCube data we are interested in.

The LQs are also interesting candidates for the explanations of anomalies in low-energy flavor physics experiments [13–15] concerning the B meson semileptonic decays that hint at the lepton flavor universality violation. The anomalies in question, i.e., $R_{D^{(*)}}$ and $R_{K^{(*)}}$, test in particular the couplings of LQs to the heavy quarks and leptons and have been studied extensively in the context of both scalar [16–20] and vector [19, 21–24] LQs. The LQ couplings to the leptons and the light quarks are constrained through the studies of the LQ production and subsequent decay in a number of collider experiments. Prior to the LHC era, the LQs were searched for at LEP [25], HERA [26, 27] and Tevatron [28, 29]. The LHC collaborations have looked for the LQs mostly in the pair production processes [30–32] and have placed very stringent limits on the LQ masses. The direct search bounds at the colliders are usually model dependent since they rely on the ansatz for the underlying flavor structure. For a summary of currently available bounds on the LQ masses and couplings from the LHC searches for different flavor final states see, for example, Refs. [33, 34].

The IceCube data offers an independent way to constrain the LQ mass m_{LQ} and its couplings that we want to explore. If the centre-of-mass energy of the incoming high energy PeV neutrino of energy E_ν colliding with

the nucleon of mass m_N at rest is sufficiently large, i.e., for $\sqrt{2m_N E_\nu} \geq m_{LQ}$, it can trigger a resonant s -channel LQ exchange. This in turn leads to a deviation of the neutrino-nucleon cross section from the SM one and can thus potentially explain the observed high-energy PeV events by improving the overall fit of the measured event rate. The resonant production has been studied in literature through the scalar LQ interaction with specific generations of both quarks and leptons. The interaction of scalar LQs R_2 , \tilde{R}_2 , and S_3 with the quarks of the first generation and the leptons of the first and second generations has been studied in Refs. [35–37]. Since the scalar LQ mass and its couplings with the first generation quarks and leptons are strongly constrained by the LHC as well as the atomic parity violation (APV) experiments a lot of studies have been done for the scalar LQ interaction between the first generation quarks and the third generation lepton [38–40]. In order to simultaneously explain the B -physics anomalies, the scalar LQ scenario where R_2 couples the heavy quark flavors with the third generation leptons is studied in Ref. [41]. There is also an earlier study [42] in the context of $SU(2)$ singlet LQ with couplings to either the second or third generation quarks or leptons focusing on the use of the inelasticity distribution of the events as an important tool for revealing the effects of NP. An R-parity violating supersymmetric model including squark resonances has also been considered to address the IceCube data [43].

In this work we study the implications of two SM $SU(2)$ singlet LQs, S_1 and U_1 , on the ultra high-energy neutrino spectrum at IceCube. We perform a thorough analysis of the S_1 scenario assuming non-zero couplings between S_1 , down quark, and neutrinos of all three generations while taking into account the fact that the S_1 couplings to the first generation quarks and e and/or μ are strongly constrained by the LHC direct searches, the leptonic pseudoscalar decay measurements, and, in the e case, by the APV experiments. There already exists an analysis that pursues the effect of S_1 on the IceCube data. Namely, the PeV astrophysical neutrino events are addressed with the S_1 mass of 600–650 GeV and the presence of only ν_τ -nucleon collision in Ref. [39]. Note, however, that the LQ masses and the associated couplings considered in Ref. [39] to explain the PeV events are ruled out by both the current LHC data and the low-energy flavor experiments.

We also study the vector LQ U_1 scenario assuming non-zero Yukawa couplings between the down quark and the charged leptons. Consequentially, U_1 couples up-type quarks to neutrinos. This is qualitatively different from the S_1 case where S_1 couples down quark to neutrinos. We, in particular, study couplings of U_1 with electrons only so as to highlight the interference between U_1 and the SM and to simplify the computation of the rate of PeV neutrino events arising from U_1 . The inclusion of the second and third generation leptons primarily dilutes the required interference effect resulting in an inferior fit to data. The analysis done in the context of U_1 is technically very similar to the S_1 case. The expected rate of events from both S_1 and U_1 is computed and added to the SM expectation to determine the masses and the couplings currently allowed by the observed spectrum at the IceCube. We take into account for both scenarios the whole IceCube energy range, i.e., 10 TeV–10 PeV, and initially include in the numerical analysis only those bins in which events have been observed. We subsequently perform the analysis that includes the zero-event bins. Since the observed neutrino rate at the IceCube is proportional to the neutrino-nucleon cross section we also consider the introduction of couplings between LQs, the quarks, and the right-handed neutrinos and investigate associated effects. The right-handed neutrinos are assumed to be light and are only produced in the final state.

The outline of the paper is as follows. We describe the two LQ scenarios considered in our work in Sec. 2. We then discuss the neutrino-nucleon cross section for S_1 and U_1 in Sec. 3 followed by the data analysis of the IceCube PeV events within this framework in Sec. 4. The constraints from the low-energy experiments on these LQ scenarios are considered in Sec. 5. The combined analysis using the IceCube data along with the LHC results and the low-energy flavor observables for both S_1 and U_1 is presented in Sec. 6. Finally we conclude in Sec. 7.

2 Leptoquark Scenarios

We briefly review in this section the LQ scenarios we consider in this work. The two scenarios used for our analysis are the scalar LQ S_1 and the vector LQ U_1 .

2.1 Scalar leptoquark $S_1 = (\bar{\mathbf{3}}, \mathbf{1}, 1/3)$

We study the effects of S_1 , whose $SU(3) \times SU(2) \times U(1)$ quantum numbers are $(\bar{\mathbf{3}}, \mathbf{1}, 1/3)$, on the IceCube observables. In our normalisation the electric charge of S_1 is $1/3$ in the absolute units of the electron charge. In the mass eigenstate basis, the relevant Lagrangian terms are of the form

$$\mathcal{L} \supset -(y^L U)_{1j} \bar{d}_L^C S_1 \nu_L^j + (V^* y^L)_{ij} \bar{u}_L^C S_1 e_L^j + y_{1j}^R \bar{d}_R^C S_1 \nu_R^j + \text{h.c.}, \quad (2.1)$$

where the subscripts $i, j (= 1, 2, 3)$ denote the flavor of the quarks and leptons, V is the Cabibbo-Kobayashi-Maskawa (CKM) mixing matrix and U is the Pontecorvo-Maki-Nakagawa-Sakata (PMNS) mixing matrix. We work under the assumption that the only non-zero S_1 couplings are $y_{11}^L \equiv y_{d\nu_e}^L$, $y_{12}^L \equiv y_{d\nu_\mu}^L$, and $y_{13}^L \equiv y_{d\nu_\tau}^L$. Since the IceCube is insensitive to the neutrino chirality we also entertain the possibility that the right-handed neutrinos are produced in the final state, with the couplings $y_{11}^R \equiv y_{d\nu_e}^R$, $y_{12}^R \equiv y_{d\nu_\mu}^R$, and $y_{13}^R \equiv y_{d\nu_\tau}^R$ being equal to each other, if and when switched on. All the other LQ Yukawa couplings are set to zero. Note that the S_1 couplings with the up-type quarks and charged leptons are fixed by the CKM mixing matrix. Since we are interested in the neutrino-nucleon cross section we find that the only relevant contributions come from the first generation quarks. For example, the contribution from both the second and the third generations of down-type quarks results in an increase of the ν - N cross section by at most 10% for an optimistic case of unit value for all the couplings, unrealistically low LQ mass m_{LQ} of around 400 GeV and $E_\nu > 10^6$ GeV.

2.2 Vector leptoquark $U_1 = (3, 1, 2/3)$

The relevant Lagrangian terms for the U_1 LQ in the mass eigenstate basis are

$$\mathcal{L} \supset (V^\dagger \chi^L U)_{ij} \bar{u}_L^i \gamma^\mu U_{1,\mu} \nu_L^j + \chi_{1j}^L \bar{d}_L^1 \gamma^\mu U_{1,\mu} e_L^j + \chi_{1j}^R \bar{u}_R^1 \gamma^\mu U_{1,\mu} \nu_R^j + \text{h.c.} \quad (2.2)$$

We consider the scenario where U_1 only couples with the down quark and charged leptons of all three generations with

$$\chi_{11}^L \equiv \chi_{de}^L, \quad \chi_{12}^L \equiv \chi_{d\mu}^L, \quad \chi_{13}^L \equiv \chi_{d\tau}^L. \quad (2.3)$$

We also analyse the possibility when the couplings $\chi_{11}^R \equiv \chi_{u\nu_e}^R$, $\chi_{12}^R \equiv \chi_{u\nu_\mu}^R$, and $\chi_{13}^R \equiv \chi_{u\nu_\tau}^R$ of U_1 with the up quark and the right-handed neutrinos are switched on and equal to each other. All other U_1 couplings are set to zero.

3 Neutrino-nucleon differential cross sections

The neutrino-nucleon scattering in the SM gives rise to the charged current ($\nu_\ell N \rightarrow \ell X$) and the neutral current ($\nu_\ell N \rightarrow \nu_\ell X$) interactions mediated by W and Z bosons, respectively. The target nucleon N is an isoscalar nucleon with $N = (n + p)/2$, X is the hadronic final state, and $\ell = e, \mu, \tau$. The SM differential cross sections in terms of the scaling variables are given as

$$\frac{d^2 \sigma_{\nu N}^{\text{CC}}}{dx dy} = \frac{2G_F^2 m_N E_\nu}{\pi} \left(\frac{m_W^2}{Q^2 + m_W^2} \right)^2 [xq(x, Q^2) + x\bar{q}(x, Q^2)(1 - y)^2], \quad (3.1)$$

$$\frac{d^2 \sigma_{\nu N}^{\text{NC}}}{dx dy} = \frac{G_F^2 m_N E_\nu}{2\pi} [xq^0(x, Q^2) + x\bar{q}^0(x, Q^2)(1 - y)^2], \quad (3.2)$$

where $-Q^2$ is the invariant momentum-square transfer to the exchanged vector boson, m_N and $m_{W(Z)}$ are the nucleon and intermediate $W(Z)$ boson masses, respectively, and $G_F = 1.166378 \times 10^{-5} \text{ GeV}^{-2}$ is the Fermi coupling constant. The differential distributions in Eqs. (3.1) and (3.2) are with respect to the Bjorken scaling variable x and the inelasticity parameter y , where

$$x = \frac{Q^2}{2m_N y E_\nu} \quad \text{and} \quad y = \frac{E_\nu - E_\ell}{E_\nu}, \quad (3.3)$$

with E_ℓ denoting the energy carried away by the outgoing lepton or the neutrino in the laboratory frame and x is the fraction of the initial nucleon momentum taken by the struck quark. Here, $q(x, Q^2)$ and $\bar{q}(x, Q^2)$ ($q^0(x, Q^2)$ and $\bar{q}^0(x, Q^2)$) are respectively the quark and anti-quark density distributions in a proton, summed over valence and sea quarks of all flavors relevant for CC (NC) interactions:

$$q(x, Q^2) = \frac{u_v(x, Q^2) + d_v(x, Q^2)}{2} + \frac{u_s(x, Q^2) + d_s(x, Q^2)}{2} + s_s(x, Q^2) + b_s(x, Q^2), \quad (3.4)$$

$$\bar{q}(x, Q^2) = \frac{u_s(x, Q^2) + d_s(x, Q^2)}{2} + c_s(x, Q^2) + t_s(x, Q^2), \quad (3.5)$$

$$q^0(x, Q^2) = \left(\frac{m_Z^2}{Q^2 + m_Z^2} \right)^2 \left[\left(\frac{u_v(x, Q^2) + d_v(x, Q^2)}{2} + \frac{u_s(x, Q^2) + d_s(x, Q^2)}{2} \right) (L_u^2 + L_d^2) \right. \\ \left. + \frac{u_s(x, Q^2) + d_s(x, Q^2)}{2} (R_u^2 + R_d^2) + (s_s(x, Q^2) + b_s(x, Q^2))(L_d^2 + R_d^2) \right]$$

$$+ (c_s(x, Q^2) + t_s(x, Q^2))(L_u^2 + R_u^2) \Big], \quad (3.6)$$

$$\begin{aligned} \bar{q}^0(x, Q^2) = & \left(\frac{m_Z^2}{Q^2 + m_Z^2} \right)^2 \left[\left(\frac{u_v(x, Q^2) + d_v(x, Q^2)}{2} + \frac{u_s(x, Q^2) + d_s(x, Q^2)}{2} \right) (R_u^2 + R_d^2) \right. \\ & + \frac{u_s(x, Q^2) + d_s(x, Q^2)}{2} (L_u^2 + L_d^2) + (s_s(x, Q^2) + b_s(x, Q^2))(L_d^2 + R_d^2) \\ & \left. + (c_s(x, Q^2) + t_s(x, Q^2))(L_u^2 + R_u^2) \right], \end{aligned} \quad (3.7)$$

with the chiral couplings given by $L_u = 1 - (4/3)x_W$, $L_d = -1 + (2/3)x_W$, $R_u = -(4/3)x_W$, and $R_d = (2/3)x_W$, where $x_W = \sin^2 \theta_W$ and θ_W is the weak mixing angle. For the $\bar{\nu}N$ cross sections Eqs. (3.1) and (3.2) are the same but with each quark distribution function replaced by the corresponding anti-quark distribution function, and vice-versa, i.e., $q(x, Q^2) \leftrightarrow \bar{q}(x, Q^2)$, $q^0(x, Q^2) \leftrightarrow \bar{q}^0(x, Q^2)$. The parton distribution functions (PDFs) of the quarks are evaluated at energy Q^2 , and the Mathematica package MSTW [44] is used throughout this work.

There are also neutrino-electron interactions, but they can be generally neglected with respect to the neutrino-nucleon cross section because of the smallness of electron's mass, except for the resonant formation of the intermediate W^- boson in the $\bar{\nu}_e e$ interactions at around $E_\nu = m_W^2/(2m_e) = 6.3 \times 10^6$ GeV, known as the Glashow resonance. The differential cross sections for all the neutrino electron reactions are listed in Ref. [45]. The total neutrino-nucleon cross section is obtained by integrating the differential cross sections in Eqs. (3.1) and (3.2) over the x and y variables:

$$\sigma(E_\nu) \equiv \int_0^1 \int_0^1 dx dy \frac{d^2\sigma}{dx dy}. \quad (3.8)$$

We show in Fig. 1 the integrated SM cross sections for the CC and NC neutrino-nucleon scatterings, the neutrino-electron interactions and antineutrino-electron scattering. At the IceCube detector the neutrinos

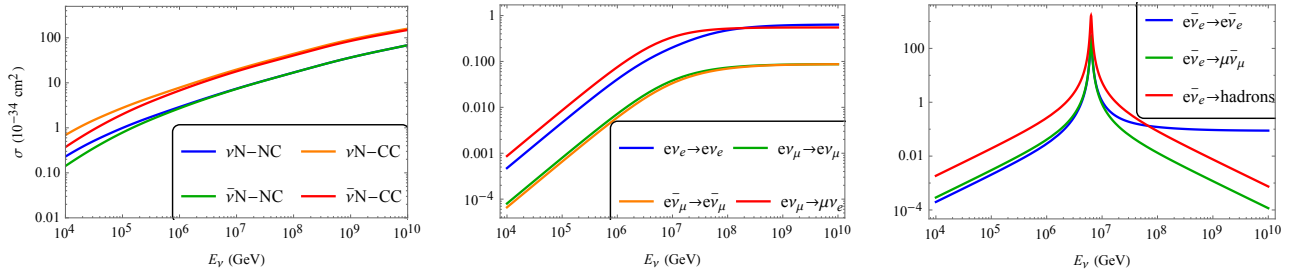


Figure 1: The neutrino-induced scattering cross sections, σ (10^{-34} cm 2) in the SM case, as a function of the incoming neutrino energy E_ν .

interact with the nucleons present in the ice. We assume that the natural ice nucleus is close enough to be considered as an isoscalar with 10 protons and 8 neutrons.

The LQ S_1 mediates the NC interactions $\nu_\ell d \rightarrow \nu_\ell d$ and $\nu_\ell d \rightarrow \nu_{\ell'} d$ and the CC interactions $\nu_\ell \bar{u} \rightarrow \ell \bar{d}$, $\nu_\ell \bar{u} \rightarrow \ell' \bar{d}$, and $d \nu_\ell \rightarrow u \ell$, $d \nu_\ell \rightarrow u \ell'$, where $\ell \neq \ell'$. The Feynman diagrams for the relevant processes are shown in Fig. 2. The charm contribution towards the t -channel CC process depicted in Fig. 2(iii), due to small PDFs, is maximally around 0.001% for the choice of the mass and the couplings considered here and therefore neglected. The differential $\nu_j N$ cross sections in the presence of the S_1 interaction are given by

$$\begin{aligned} \frac{d^2\sigma_{\nu_j N}^{CC}}{dx dy} = & \frac{m_N E_\nu}{16\pi} |(y^L U)_{1j}|^2 \left[\sum_{k=1}^3 |(V^* y^L)_{1k}|^2 \right] \left(\frac{1}{|2xm_N E_\nu - m_{S_1}^2 + i\Gamma_{S_1} m_{S_1}|^2} \right. \\ & \left. \left[\frac{u_v + d_v}{2} + \frac{u_s + d_s}{2} \right] + \frac{1}{(Q^2 - 2xm_N E_\nu - m_{S_1}^2)^2} (1-y)^2 \frac{u_s + d_s}{2} \right), \end{aligned} \quad (3.9)$$

$$\begin{aligned} \frac{d^2\sigma_{\nu_j N}^{NC}}{dx dy} = & \frac{m_N E_\nu}{16\pi} |(y^L U)_{1j}|^2 \left[\sum_{k=1}^3 |(y^L U)_{1k}|^2 + \sum_{k=1}^3 |y_{1k}^R|^2 \right] \left(\frac{1}{|2xm_N E_\nu - m_{S_1}^2 + i\Gamma_{S_1} m_{S_1}|^2} \right. \\ & \left. \left[\frac{u_v + d_v}{2} + \frac{u_s + d_s}{2} \right] + \frac{1}{(Q^2 - 2xm_N E_\nu - m_{S_1}^2)^2} (1-y)^2 \frac{u_s + d_s}{2} \right), \end{aligned} \quad (3.10)$$

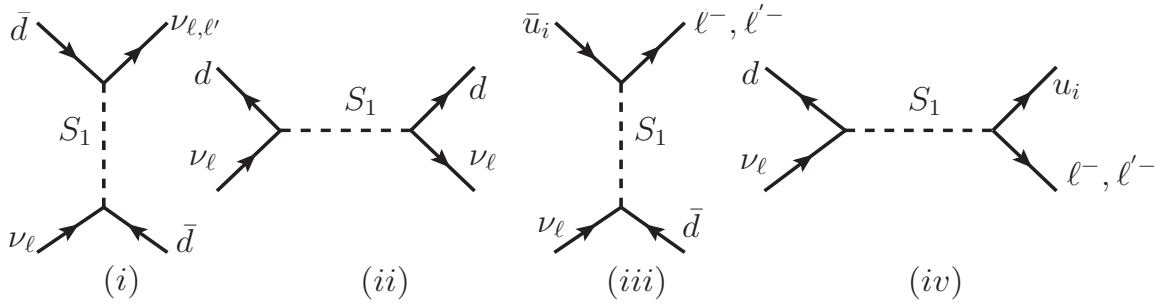


Figure 2: The relevant Feynman diagrams for the neutrino-quark interactions mediated by the scalar LQ S_1 .

where $j = 1, 2, 3$ and Γ_{S_1} is the decay width of S_1 given by

$$\Gamma_{S_1} = \frac{m_{S_1}}{16\pi} \left[\sum_{i=1}^3 |(y^L U)_{1i}|^2 + \sum_{i,j=1}^3 |(V^* y^L)_{ij}|^2 + \sum_{i=1}^3 |y_{1i}^R|^2 \right]. \quad (3.11)$$

Note that the effect of the right-handed couplings to the neutrinos is only visible in NC interactions.

The U_1 LQ, similarly to the S_1 case, contributes to both the NC and CC interactions. The possible contributing Feynman diagrams in the presence of U_1 are shown in Fig. 3. The u_i in Fig. 3 represents the contributions from all three generations of up-type quarks. Note, however, that the charm contributions towards the NC processes, due to small PDFs, are of the order of 0.001% and can be safely neglected. The modified

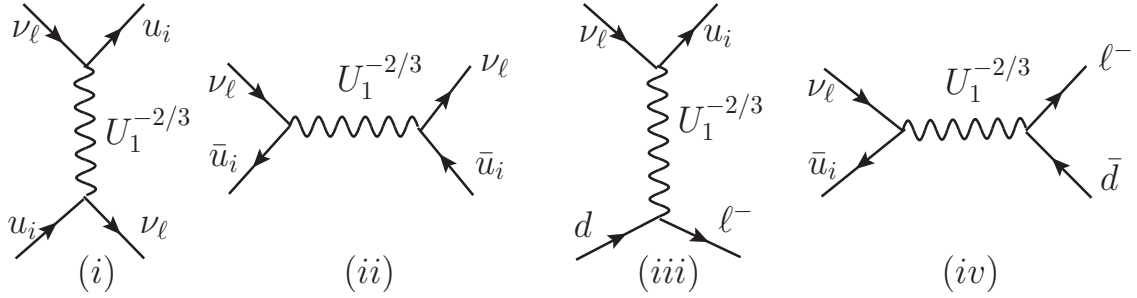


Figure 3: The relevant Feynman diagrams for the neutrino-quark interactions mediated by the vector LQ U_1 .

$q^0(x, Q^2)$ and $\bar{q}^0(x, Q^2)$ listed in Eqs. (3.6), (3.7), in the presence of U_1 , are given below.

$$q^0(x, Q^2) = \left(\frac{m_Z^2}{Q^2 + m_Z^2} \right)^2 \left[\left(\frac{u_v(x, Q^2) + d_v(x, Q^2)}{2} + \frac{u_s(x, Q^2) + d_s(x, Q^2)}{2} \right) L_d^2 + \frac{u_s(x, Q^2) + d_s(x, Q^2)}{2} (R_u^2 + R_d^2) \right] + \left[\frac{u_v(x, Q^2) + d_v(x, Q^2)}{2} + \frac{u_s(x, Q^2) + d_s(x, Q^2)}{2} \right] \left| \frac{m_Z^2}{Q^2 + m_Z^2} L_u + \frac{|(V^\dagger \chi^L U)_{1i}|^2}{2\sqrt{2}G_F} \frac{1}{Q^2 - 2xM_N E_\nu - m_{U_1}^2} \right|^2 \quad (3.12)$$

$$\bar{q}^0(x, Q^2) = \left(\frac{m_Z^2}{Q^2 + m_Z^2} \right)^2 \left[\left(\frac{u_v(x, Q^2) + d_v(x, Q^2)}{2} + \frac{u_s(x, Q^2) + d_s(x, Q^2)}{2} \right) (R_u^2 + R_d^2) + \frac{u_s(x, Q^2) + d_s(x, Q^2)}{2} L_d^2 \right] + \frac{u_s(x, Q^2) + d_s(x, Q^2)}{2} \left| \frac{m_Z^2}{Q^2 + m_Z^2} L_u + \frac{|(V^\dagger \chi^L U)_{1j}|^2}{2\sqrt{2}G_F} \frac{1}{2xm_N E_\nu - m_{U_1}^2 + i\Gamma_{U_1} m_{U_1}} \right|^2 \quad (3.13)$$

where $j = 1, 2, 3$. The above equation shows the case for the same flavor neutrino in the initial and the final state which interferes with the SM contribution. There will be additional contributions from the cases where

the final state will consist of right-handed neutrinos or will have a neutrino of different flavor from the initial one and are given by

$$\begin{aligned} \frac{d^2 \sigma_{\nu_j N}^{NC}}{dx dy} &= \frac{E_\nu}{8G_F^2} |(V^\dagger \chi^L U)_{1j}|^2 \left(\frac{1}{(Q^2 - 2xm_N E_\nu - m_{U_1}^2)^2} \left(y^2 \sum_{k=1}^3 |\chi_{1k}^R|^2 + \sum_{\substack{k=1 \\ k \neq j}}^3 |(V^\dagger \chi^L U)_{1k}|^2 \right) \right. \\ &\quad \left. \left[\frac{u_v + d_v}{2} + \frac{u_s + d_s}{2} \right] + (1-y)^2 \left| \frac{1}{2xm_N E_\nu - m_{U_1}^2 + i\Gamma_{U_1} m_{U_1}} \right|^2 \sum_{\substack{k=1 \\ k \neq j}}^3 |(V^\dagger \chi^L U)_{1k}|^2 \frac{u_s + d_s}{2} \right). \end{aligned}$$

In case of CC interactions, the coefficient $m_W^2/(Q^2 + m_W^2)$ in Eq. (3.1) is modified to

$$\begin{aligned} \left(\frac{m_W^2}{(Q^2 + m_W^2)} \right)^2 q(x, Q^2) &\Rightarrow \left| \frac{m_W^2}{(Q^2 + m_W^2)} + \frac{\chi_{dj}^L (V^\dagger \chi^L U)_{1j}}{2\sqrt{2}G_F} \frac{1}{Q^2 - 2xm_N E_\nu - m_{U_1}^2} \right|^2 q(x, Q^2) \\ \left(\frac{m_W^2}{(Q^2 + m_W^2)} \right)^2 \bar{q}(x, Q^2) &\Rightarrow \left| \frac{m_W^2}{(Q^2 + m_W^2)} + \frac{\chi_{dj}^L (V^\dagger \chi^L U)_{1j}}{2\sqrt{2}G_F} \frac{1}{2xm_N E_\nu - m_{U_1}^2 + i\Gamma_{U_1} m_{U_1}} \right|^2 \bar{q}(x, Q^2), \end{aligned} \quad (3.14)$$

taking into account the interference terms only when the final state is similar to the SM. The decay width of U_1 is given by

$$\Gamma_{U_1} = \frac{m_{U_1}}{24\pi} \left[\sum_{i=1}^3 |\chi_{1i}^L|^2 + \sum_{i=1}^3 |(V^\dagger \chi^L U)_{1i}|^2 + \sum_{i=1}^3 |\chi_{1i}^R|^2 \right]. \quad (3.15)$$

The interference effect of U_1 with the SM can lead to interesting signatures if compared to the S_1 case. We show in Fig. 4 the cross sections in case of S_1 and U_1 compared to the SM for a benchmark point of $m_{S_1, U_1} = 800$ GeV, $y_{d\nu_e, d\nu_\mu, d\nu_\tau}^L = 0.5$, $\chi_{de, d\mu, d\tau}^L = 0.5$, and $y_{d\nu_e}^R, \chi_{u\nu_e}^R = 1.0$. The NC is more sensitive compared to the CC for this particular choice of the couplings. The effect of the U_1 for a given mass is more enhanced compared to S_1 at large E_ν . This is mainly due to the difference in PDFs of the initial contributing quark, i.e., u (d) quark in case of U_1 (S_1).

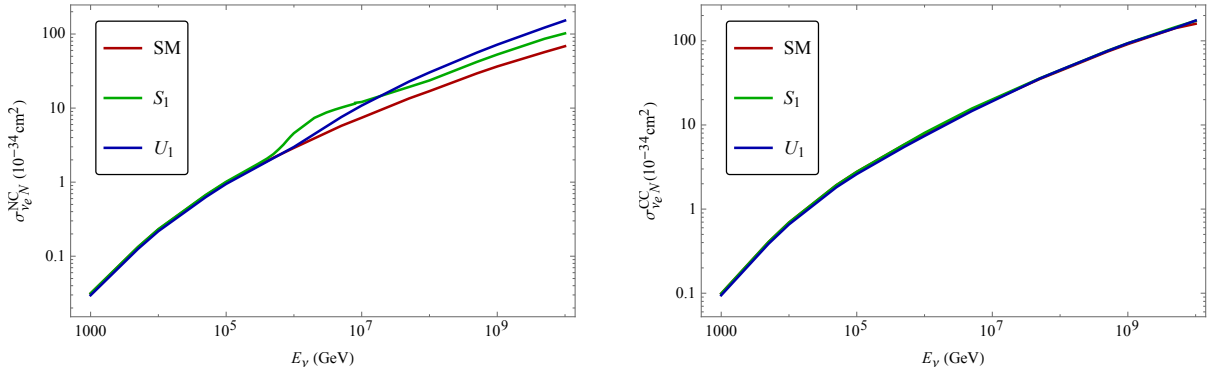


Figure 4: The neutrino-nucleon scattering cross sections for neutral current (left panel) and charged current (right panel) interactions in the SM, SM + S_1 , and SM + U_1 cases for $m_{S_1, U_1} = 800$ GeV, $y_{d\nu_e, d\nu_\mu, d\nu_\tau}^L = 0.5$, $\chi_{de, d\mu, d\tau}^L = 0.5$, and $y_{d\nu_e}^R, \chi_{u\nu_e}^R = 1.0$.

We next study in details the effects of S_1 and U_1 on the observed IceCube PeV events.

4 PeV events in IceCube

The high-energy neutrinos coming from outside the atmosphere are detected in the IceCube detector by observing the Cherenkov light emitted by the secondary charged particles produced in the interaction of the neutrinos with the nucleus present in the ice. The CC and the NC interactions have distinctive topologies depending on the flavor of the incoming neutrinos. The shower-like events are induced by CC of ν_e and ν_τ interactions and NC interactions of neutrinos of all flavors. The tracks are produced in the CC interactions of ν_μ and ν_τ (τ produced in the final state decays to $\nu_\tau \nu_\mu \mu$, giving a distinctive signature, double cascade). The expected total

number of events at the IceCube from the NC or CC interactions in the deposited energy interval $(E_{\text{dep}}^i, E_{\text{dep}}^f)$ can be written as

$$\mathcal{N}^{ch} = T N_A \int_{E_{\text{dep}}^i}^{E_{\text{dep}}^f} dE_{\text{dep}} \int_0^\infty dE_\nu \text{Att}_{\nu_\ell}^f(E_\nu) \frac{d\phi_{\nu_\ell}^f}{dE_\nu} \int_0^1 dy M_{\text{eff}}(E_{\text{true}}) R(E_{\text{true}}, E_{\text{dep}}, \sigma(E_{\text{true}})) \frac{d\sigma^{ch}(E_\nu, y)}{dy}, \quad (4.1)$$

where T is the exposure time in secs (2078 days of data taking [3]), N_A is the Avogadro's number 6.022×10^{23} , ch is the neutral or the charged channel and $M_{\text{eff}}(E_{\text{true}})$ denotes the effective mass of the detector. The effect of the earth's attenuation, in case of neutrino's energy above a few TeV, where the mean free path inside the earth becomes comparable to the distance travelled by the neutrino, is denoted by $\text{Att}_{\nu_\ell}^f(E_\nu)$. The downward events with the neutrino coming from the southern hemisphere do not interact with the earth and therefore have the 4π averaged attenuation factor given by $1/2$. On the other hand for the upward events with the neutrino coming from the northern hemisphere, the attenuation effects due to the interaction with the earth must be taken into account. The total 4π averaged attenuation factor of the astrophysical neutrinos is given by

$$\text{Att}_{\nu_\ell}^a(E_\nu) = \frac{1}{2} \left(1 + \int_0^1 \frac{F_{\nu_\ell}(E_\nu, X(\theta))}{F_{\nu_\ell}(E_\nu, 0)} d\cos\theta \right), \quad (4.2)$$

where $F_{\nu_\ell}(E_\nu, X)$ is the differential energy spectrum of the neutrinos at a column depth X of the earth, with $F_{\nu_\ell}(E_\nu, X) = d\Phi_{\nu_\ell}(E_\nu, X)/dE_\nu$. The column depth X depends on the nadir angle of the incident neutrino beam, where $\theta = 0^\circ$ corresponds to a beam transversing the diameter of the earth and is defined as the thickness of the matter transversed by the upgoing leptons. It is given by $X(\theta) = \int_0^{2R_\oplus \cos\theta} \rho(r(L)) dL$, where $R_\oplus \approx 6371$ km is the earth radius, ρ is the density of the earth given by the Preliminary Earth Model [45], and L is the neutrino beam path with $r(L)$ as the distance of the beam from the center of the earth given by $R_\oplus^2 + L^2 - 2R_\oplus L \cos\theta$. The averaged attenuation and regeneration factors for the astrophysical neutrinos and the anti-neutrinos are shown in Fig. 5 for the SM (left panel) and for a representative SM + S_1 scenario (right panel), with $m_{S_1} = 800$ GeV, $y_{d\nu_e}^L = y_{d\nu_\mu}^L = y_{d\nu_\tau}^L = 0.5$, and $y_{d\nu_\ell}^R = 1.0$.

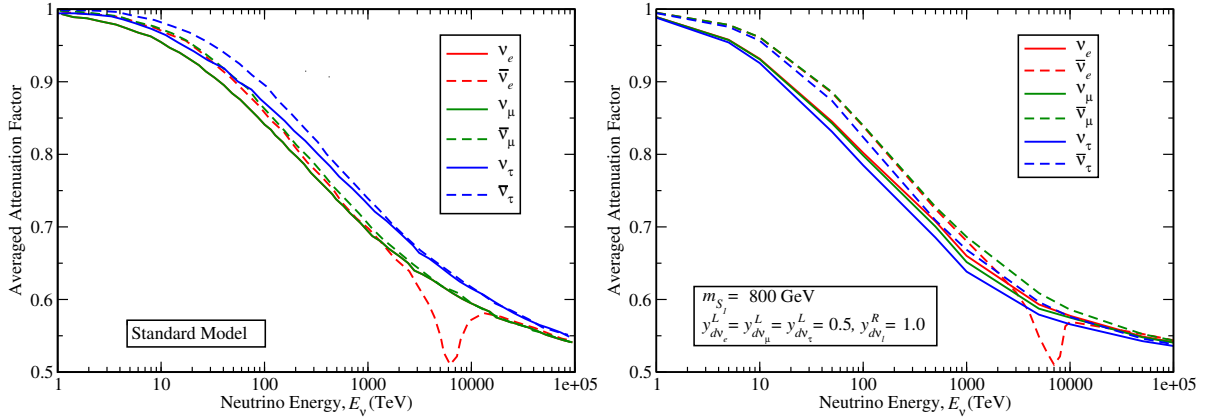


Figure 5: The averaged attenuation and the regeneration factors for the cosmic neutrinos (solid lines) and anti-neutrinos (dashed lines) travelling the earth for an isotropic power-law spectrum with $E_\nu^{-\gamma}$, with $\gamma = 2.92$. In the SM case the curves for ν_e and $\bar{\nu}_e$ are similar with that of ν_μ and $\bar{\nu}_\mu$ except for the $\bar{\nu}_e$ around the Glashow resonance.

The effective mass of the detector, $M_{\text{eff}}(E_{\text{true}})$ is a function of the true electromagnetic equivalent energy and is defined as the mass of the target material times the efficiency of converting the true deposited energy of the event into an observed signal. The energy resolution function is given by $R(E_{\text{true}}, E_{\text{dep}}, \sigma(E_{\text{true}}))$ and is represented by a Gaussian distribution. The neutrino-nucleon differential cross section for the charged and the neutral channels is given by $d\sigma^{ch}(E_\nu, y)/dy$. Finally the incoming neutrino flux is given by $d\phi_{\nu_\ell}^f/dE_\nu$, where f = astrophysical, conventional atmospheric or prompt atmospheric. The incoming astrophysical neutrino flux follows the isotropic single unbroken power-law spectrum given by [3, 46, 47]

$$\frac{d\phi_{\nu_\ell}^{\text{astro}}}{dE_\nu} = 3\Phi_0 f_\ell \left(\frac{E_\nu}{100 \text{ TeV}} \right)^{-\gamma}, \quad (4.3)$$

where f_ℓ is the fraction of neutrinos of each flavor ℓ . The fit is performed assuming a $(1/3 : 1/3 : 1/3)_\oplus$ flavor ratio, which yields the best fit value for the spectral index $\gamma = 2.92_{-0.29}^{+0.33}$, with a normalization $\Phi_0 =$

$2.46 \pm 0.8 \times 10^{-18} \text{ GeV cm}^{-2} \text{ s}^{-1} \text{ sr}^{-1}$. This flavor ratio at the earth is obtained by assuming the most commonly considered scenario where the incoming neutrino flux is dominated by the decay of pions produced in the pp and $p\gamma$ interactions. These pions and their daughter muons dominate this incoming flux resulting in a flavor ratio of $(1/3 : 2/3 : 0)$ at the source. The flavor ratio at the source, due to neutrino oscillations, averaged by the propagation over the large astronomical distances leads to $(1/3 : 1/3 : 1/3)$ ratio at the earth. The flavor ratio of the incoming neutrinos at the earth will depend on their production at the source. Recently a global fit was done in Refs. [46, 47] combining results from all the contained events in IceCube measuring the source flavor composition of the neutrinos and the best fit composition was found to be $(0 : 0.21 : 0.79)_{\oplus}$, with the other possible standard flavor compositions allowed at $<68\%$ confidence level (C.L.). The current best fit composition with more ν_{τ} obtained in the SM-only calculation, can be probably due to an underlying NP scenario leading to an enhanced ν_{τ} scattering.

The deposited energy is different for the CC and the NC interactions and is smaller than the incoming neutrino energy E_{ν} by a factor which depends on the interaction channel. In case of the NC interaction, the cross section is identical for all the neutrino flavors. The resulting hadronic shower originates from the outgoing hadron which carries a fraction of the initial neutrino energy determined by the inelasticity parameter y . The true deposited energy for the neutral channel is therefore given by

$$E_{\text{true}}^{\text{NC}} = F_h(E_{\nu}y)E_{\nu}y, \quad \text{where} \quad F_h(E_X) = 1 - 0.533 \left(\frac{E_X}{0.399 \text{ GeV}} \right)^{0.130}. \quad (4.4)$$

The true deposited energy in case of CC will be different for the different neutrino flavors and is defined in details in Ref. [48]. The calculations performed here leading to the total number of events in a given interval of deposited energy are similar to Ref. [48]. The event spectra of showers and tracks for each flavor (summing over all the neutrino and antineutrino flavors), with the values of the best fit IceCube spectra in case of the SM, are shown in Fig. 6. Since the contribution from the electron showers is the largest, the electron should be

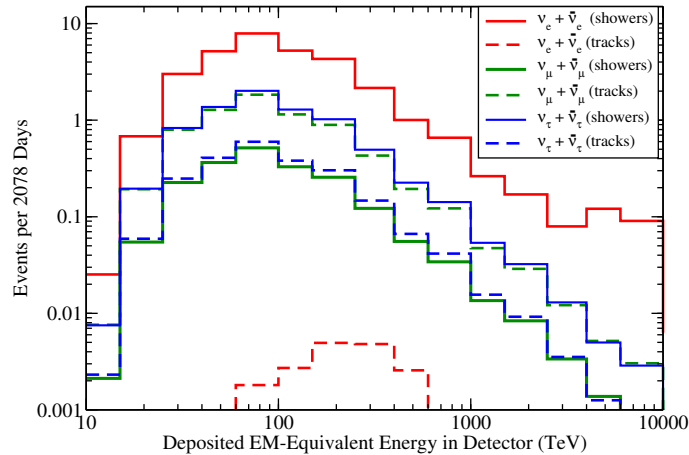


Figure 6: The event spectra from the SM in IceCube, as a function of the EM-equivalent deposited energy, of tracks and showers for each flavor after 2078 days assuming an isotropic power-law spectrum, with $(1/3 : 1/3 : 1/3)$ ratio.

sensitive to the NP effects if one is to have an enhanced effect compared to the SM. The S_1 and U_1 effect with the electron coupling switched on is thus studied first. Since the U_1 LQ interferes with the SM contribution, we show in Fig. 7 the ratio of the $\nu_e N$ total cross sections for the SM+ U_1 and the SM for different values of masses and couplings. The interference effect is clearly visible for low values of mass and large values of χ_{de}^L . The current IceCube data has less events compared to the SM in the 300–1000 TeV energy range whereas for energies greater than 1000 TeV the observed events are more compared to the SM. It can be seen from Fig. 7 that there is a crossover in the relevant energy range making it an interesting feature for a more detailed study. We would like to point out that the inclusion of $\chi_{d\mu}^L$ and/or $\chi_{d\tau}^L$ will push the crossover away from the interesting energy range. The three couplings then have to be adjusted so as to get the required effect.

We study whether the SM + LQ scenarios result in a better or a worse fit of the IceCube data compared to the SM case by calculating the percent change in χ^2 [37]. We accordingly define

$$\chi_{\text{model}}^2 = \sum_{i \geq 100 \text{ TeV}}^{\text{bins}} \frac{(N_{\text{model}_i} - N_{\text{data}_i})^2}{N_{\text{data}_i}}, \quad \delta = 100\% \times \frac{\chi_{\text{SM}}^2 - \chi_{\text{SM+LQ}}^2}{\chi_{\text{SM}}^2}, \quad (4.5)$$

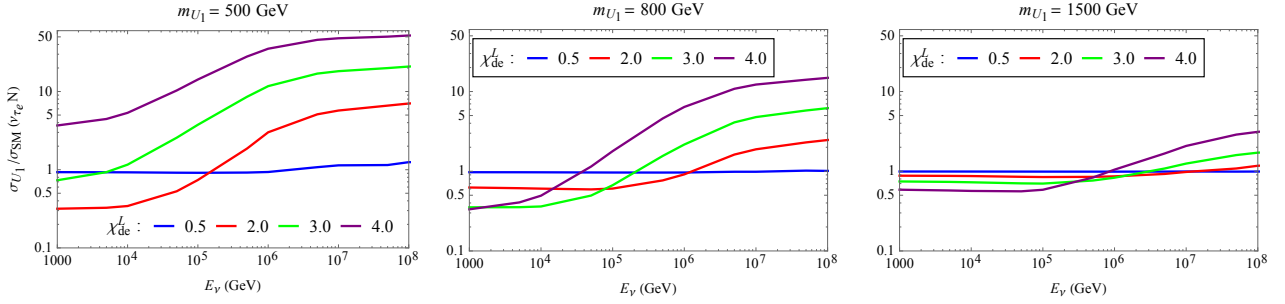


Figure 7: The ratio of ν_e - N total cross sections between the SM+ U_1 and the SM for different masses and couplings of U_1 .

where the observed number of events N_{data_i} in each bin i is compared with the LQ scenario prediction and, in our case, $\text{LQ} = S_1, U_1$. We consider the events in the neutrino deposited energy range [100 TeV, 10 PeV] that is divided in 10 logarithmic energy bins. We initially use only the data for the bins with the non-zero number of events. The parameter points for the NP scenario which result in a worse fit to the IceCube data by more than 1% compared to the SM, i.e., $\delta < -1\%$, are considered to be excluded.

The SM value with the best fit value of γ and C_0 from the IceCube data results in a χ^2 value of 9.76 and a χ^2 probability of 0.15. This shows that the current IceCube data is quite compatible with the SM. The NP contribution to the number of events in each bin depends on the values of $y_{d\nu_e, d\nu_\mu, d\nu_\tau}^L$, $y_{d\nu_e}^R$, and m_{S_1} ($\chi_{de, d\mu, d\tau}^L$, $\chi_{\nu\nu_e}^R$, and m_{U_1}) in the S_1 (U_1) case. Since the S_1 contribution adds to the SM, a small mass and a large value for the LQ-neutrino-quark coupling will lead to an enhanced number of events in each bin. This is beneficial for (detrimental to) the bins where there is an observed excess (lack) of events compared to the SM case. The minimum χ^2 in the S_1 case is achieved for the NP couplings equal to zero, which means that the S_1 events spoil the overall fit. As the total spectrum of events has a worse χ^2 fit with the inclusion of S_1 , we can rule out some parts of parameter space of this LQ scenario with the IceCube events. We show in Fig. 8 the regions in the m_{S_1} - $y_{d\nu_e}^L$ plane which result in a fit worse than SM in excess of 1%, 3%, and 5%. The hatched region above the blue line is currently excluded by the APV results. The limit on $y_{d\nu_e}^L$ from IceCube under the 1% disagreement assumption and for $m_{S_1} < 600$ GeV is comparable to the APV limits and even a bit better for masses below 400 GeV. Since the low mass region is already ruled out by the LHC searches we, in the rest of our numerical analysis, take $y_{d\nu_e}^L \leq 0.52 \times m_{S_1}/(1 \text{ TeV})$ in order to incorporate a 2σ agreement between the SM and the experimental results on APV. The percent change in χ^2 in case of U_1 is shown in Fig. 9 for the m_{U_1} - χ_{de}^L parameter space. It can be seen from Fig. 9 that the U_1 LQ of mass around 900–1000 GeV, with $\chi_{de}^L \approx 2.0$ can give a 16% improvement to the SM only fit. We find that the couplings needed for such an improvement in case of $m_{U_1} > 1.5$ TeV are close to perturbativity limit and we do not consider them here. The limit on χ_{de}^L from APV, i.e., $\chi_{de}^L \leq 0.34 \times m_{U_1}/(1 \text{ TeV})$, as a function of m_{U_1} is shown by the blue dotted line, with the region above the line being excluded. The parameter space which survives the APV constraint yields δ that is in -2% to -1% range.

The plot in Fig. 10 shows the currently allowed region by the IceCube data in the $y_{d\nu_\mu}^L$ - $y_{d\nu_\tau}^L$ plane for different values of m_{S_1} and $y_{d\nu_e}^L = 0.52 \times m_{S_1}/(1 \text{ TeV})$. The region above the relevant curves results in negative values of δ , where $\delta < -1\%$, and is therefore currently disfavoured. The weakening of the bound on the allowed coupling for larger LQ mass is expected since the LQ contribution decreases with increasing m_{S_1} resulting in larger values of couplings being viable. The S_1 contribution is added on top of the SM expected rate of events, therefore the event distributions lead to enhanced events between the 300 TeV and 1000 TeV bins, where the SM + atmospheric contribution is already above the observed spectrum. The LQs with low mass and large couplings contribute the most to this bin and are therefore excluded as they result in larger χ^2 compared to SM. The U_1 LQ can produce both shower and muon track events, but in our analysis, for the sake of simplicity we assume $\chi_{d\mu}^L = \chi_{d\tau}^L = 0$. We have also shown in Fig. 7 that the inclusion of $\chi_{d\mu}^L$ and/or $\chi_{d\tau}^L$ does not yield any additional insight and we therefore opt not to perform it in case of U_1 . Therefore U_1 only interacts through ν_e , with both CC and NC interactions leading only to showers.

The couplings of the LQs S_1 and U_1 with the right-handed neutrinos are first fixed to zero, for simplicity. We later discuss the impact of these couplings on the final event rate. The LQ interactions can in general affect the atmospheric neutrino detection rate as the atmospheric background is mostly dominated by the ν_μ induced events. We have checked that, for the choice of the couplings considered here, the atmospheric background remains unaffected. The IceCube data points, as well as the background due to atmospheric neutrinos and muons, are taken from Ref. [3]. In the presence of LQ, the source flavor composition and the flux of the neutrinos

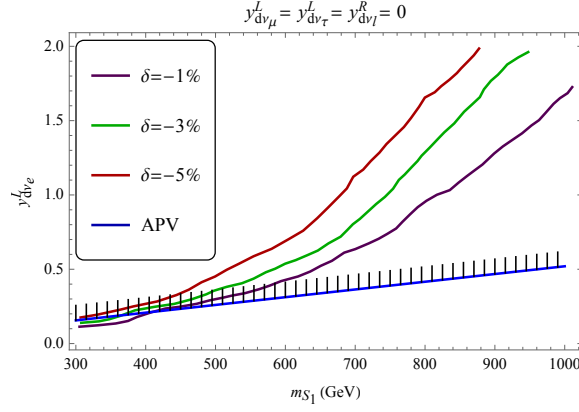


Figure 8: The region above the lines in the m_{S_1} - $y_{d\nu_e}^L$ plane resulting in a worse χ^2 compared to the SM by more than 1%, 3% and 5%. All other couplings are considered to be zero. The region above the blue line is currently excluded by the APV experiments.

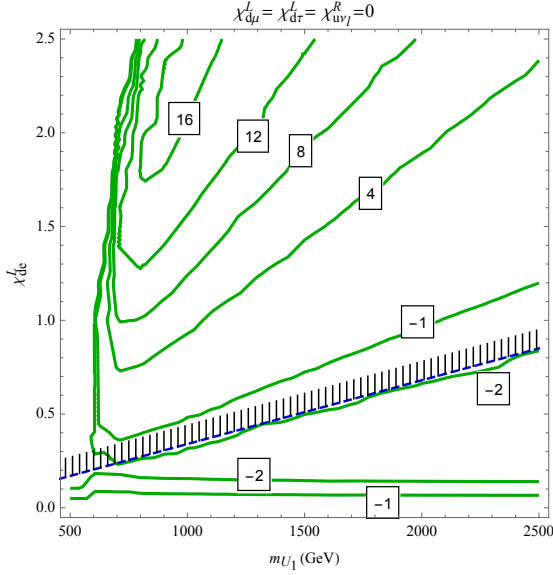


Figure 9: The contours of constant δ show the percent change in χ^2 from the SM value in m_{U_1} - χ_{de}^L parameter space. An improvement of χ^2 by about 16% compared to the SM can be obtained for $m_{U_1} \approx 900$ GeV and $\chi_{de}^L \approx 2$. The contours with negative value result in a worse fit compared to the SM case.

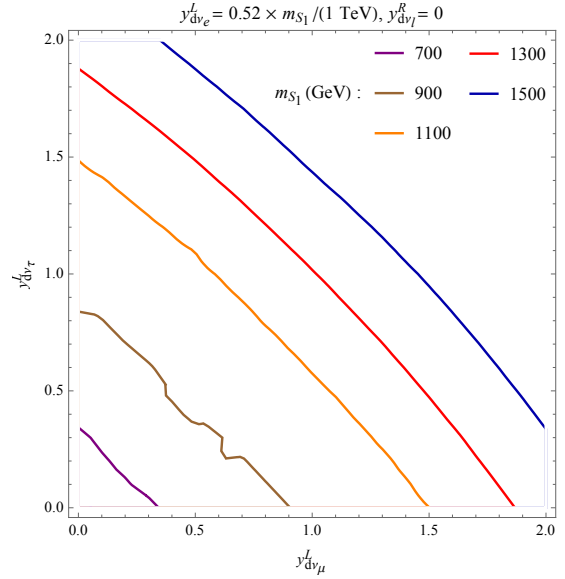


Figure 10: The lines of constant δ showcase the upper limit in $y_{d\nu_\mu}^L$ - $y_{d\nu_\tau}^L$ plane for different LQ masses, having their χ^2 value comparable to SM. The region above the line results in a fit worse than SM by 1% or more. The LQ coupling to the first generation fermions is fixed to a 2σ agreement with APV.

are expected to be modified. However, for the values of the LQ mass and the couplings considered here, the NP effect is expected to be small when compared to the SM weak interactions. The resonant production of the LQ in the s -channel for an appropriate range of incoming energy only leads to an enhancement effect in the IceCube. Thus, taking into account the flux uncertainty will lead to an equal effect in case of both the SM and the SM+LQ cases, keeping the ratio between the NP events and the SM events same. Therefore we use the value of the IceCube best fit for the flux.

We next discuss the constraints on the S_1 and U_1 parameter spaces from the low-energy flavor experiments and the LHC to see how they compare with the IceCube ones.

5 Low-energy constraints

The LQ interactions defined in the previous section can lead to leptonic decays of pseudoscalar mesons or flavor changing processes at both the tree and one-loop levels. The LQ couplings to the first generation quarks and electron are strongly constrained by APV experimental results. The experimental upper bounds on the

$\ell \rightarrow \ell' \gamma$ decay branching ratios, with the LQ contribution coming in loop, will also constrain the couplings of S_1 with the quarks and leptons. These branching ratios receive contribution from both the left-handed as well as the right-handed couplings of the quarks to the leptons. The upper limits on the lepton flavor violating decays of the μ and the τ lepton are obtained from various experiments with $\text{BR}(\mu \rightarrow e \gamma) < 4.2 \times 10^{-13}$ [49], $\text{BR}(\tau \rightarrow e \gamma) < 3.3 \times 10^{-8}$, and $\text{BR}(\tau \rightarrow \mu \gamma) < 4.4 \times 10^{-8}$ [50] @ 90% C.L.. The S_1 LQ also contributes at tree level to the rare flavor process $D^0 \rightarrow \mu^+ \mu^-$. The most recent measurement of this branching ratio comes from LHCb [51] and reads $\text{BR}(D^0 \rightarrow \mu^+ \mu^-) < 7.6 \times 10^{-9}$. The same couplings contribute to the $D^0 - \bar{D}^0$ oscillations. Following the study of the LQ effects in the $D^0 - \bar{D}^0$ oscillations explained in detail in Refs. [12, 52], we have checked that the LQ contributions are smaller than the current bounds on the $D^0 - \bar{D}^0$ mixing amplitude.

Since the LQ in our case yields new contributions to $\ell \rightarrow \ell' \gamma$, the APV measurements, the rare meson decays, and the ratio of the leptonic decays of the pseudoscalar meson, we take into account all these constraints.

Lepton flavor violation in the Pion sector

The contribution of weak singlets S_1 and U_1 to the pion muonic decays is different from the pion electron decays due to the different values of e and μ couplings with the first generation quarks as well as the dependence on m_e and m_μ . The effects of this type can be exposed by the lepton flavor universality ratios $R_{e/\mu}^\pi$ and $R_{\tau/\mu}^\pi$, where

$$R_{e/\mu}^\pi = \frac{\text{BR}(\pi^- \rightarrow e^- \bar{\nu})}{\text{BR}(\pi^- \rightarrow \mu^- \bar{\nu})}, \quad R_{\tau/\mu}^\pi = \frac{\text{BR}(\tau^- \rightarrow \pi^- \bar{\nu})}{\text{BR}(\tau^- \rightarrow \mu^- \bar{\nu})}, \quad (5.1)$$

with the experimental result $R_{e/\mu}^\pi|_{\text{exp}} = (1.2327 \pm 0.0023) \times 10^{-4}$ and the SM value $R_{e/\mu}^\pi|_{\text{SM}} = (1.2352 \pm 0.0001) \times 10^{-4}$ [53] (see Eq. (A.2)). The measured ratio is $R_{\tau/\mu}^\pi|_{\text{exp}} = 0.1082 \pm 0.0005$ [54], while the SM value is found to be $R_{\tau/\mu}^\pi|_{\text{SM}} = 0.1088 \pm 0.0002$, using Eq. (A.2).

The formulas for the branching ratios of the pion, D^0 meson and the τ lepton, in the case of S_1 and U_1 , along with the numerical values of input parameters used for our analysis are listed in the Appendix A. We next perform a randomized scan on the parameter space $m_{S_1} \in (300 \text{ GeV}, 1.5 \text{ TeV})$, $y_{d\nu_e}^L, y_{d\nu_\mu}^L, y_{d\nu_\tau}^L \in (0.0, 2.0)$ in case of S_1 and $m_{U_1} \in (300 \text{ GeV}, 2.5 \text{ TeV})$, $\chi_{de}^L, \chi_{d\mu}^L, \chi_{d\tau}^L \in (0.0, 2.0)$ in case of U_1 , taking into account the constraints from the pion sector, APV, the rare radiative decays $\ell \rightarrow \ell' \gamma$, and $D^0 \rightarrow \mu^+ \mu^-$ decays. The plots in Fig. 11 show the currently allowed parameter space of the left-handed couplings as a function of mass. The flavor experiments constrain the parameter space of the vector LQ more tightly than that of the scalar one. The S_1 LQ also contributes at loop level to the $Z \rightarrow \ell \bar{\ell}$ decay amplitude, with S_1 and the up-type quarks running in the loop. The Z branching ratio to a pair of leptons has been precisely measured in LEP [54], thereby imposing constraints on the S_1 parameter space. We have used formula for the one-loop contribution of S_1 computed in Ref. [55] and found that the bounds on the LQ couplings from the Z leptonic branching ratio is not up to par with the other experimental constraints considered before. The loop level contribution to the $Z \rightarrow \ell \bar{\ell}$ decay amplitude in case of U_1 is also negligible for the parameter space that survives the other low-energy flavor experiments.

We next discuss the LHC limits on the LQ masses and their couplings and combine the results from IceCube as well as the flavor experiments.

6 Combined analysis of the IceCube data, LHC results, and low-energy flavor physics measurements

Our goal is to combine the LHC constraints on the weak singlet scalar and vector LQs considered in our work with the IceCube data and low-energy flavor physics measurements. The LQs have been hunted for at the LHC mainly through pair-production, single production, and through dilepton and monolepton Drell-Yan process searches. Dedicated studies have been performed at the LHC, assuming LQ pair production and a 100% branching ratio (BR) of LQ decaying into a charged lepton and jet ($jj\ell^+\ell^-$, where $\ell = e, \mu$) or to jet and missing energy ($jj\nu\nu$). LQs coupling to first-generation quarks and electrons or muons are also sought in single production processes, i.e., $pp \rightarrow \ell^+\ell^-j$ [56]. Recently it was also shown that stringent limits can be obtained on LQs that couple to the first generation quarks and left-handed electrons and muons through the monolepton searches [57]. The final states relevant for our analysis are $jjee$, $jj\mu\mu$, and $jj\nu\nu$, with $j\nu$ having the dominant branching ratio. The upper limits on the LQ production cross section times BR^2 for these final states are provided by the LHC collaborations [30, 58, 59].

We show in Fig. 12 the allowed parameter space for different choices of values of relevant couplings of S_1 as a function of m_{S_1} . The parameter space allowed by the LHC is represented by the meshed region and the green shaded region is the one that results in a similar fit as the SM prediction of the IceCube data up to the

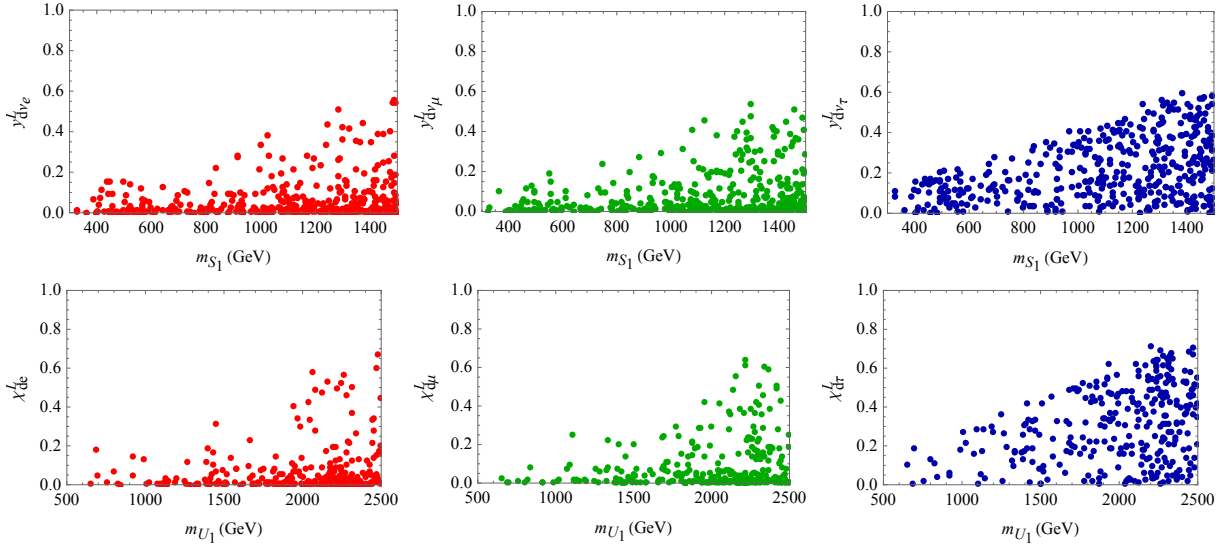


Figure 11: The allowed parameter space after taking into account the results from the most relevant low-energy experiments.

1% disagreement level. The constraints from the low-energy experiments discussed in Sec. 5 are also considered and shown by pink dots. We first assume the coupling of S_1 to down quark and ν_e to be in accordance with APV and show in Fig. 12a the allowed parameter space as a function of m_{S_1} considering $y^L_{d\nu_\mu} = y^L_{d\nu_\tau}$. The region currently in disagreement at the 1% level or less with the SM fit of the IceCube data is comparable to the LHC results for the LQ mass below 1 TeV. The considered value of $y^L_{d\nu_e} \approx 0.52 \times m_{S_1}/(1 \text{ TeV})$ leads to an enhanced effect resulting in more number of events compared to the SM. Therefore the associated χ^2 value is enhanced leading to negative δ . The absence of the LQ coupling with the electron will make the IceCube data less sensitive to the S_1 LQ parameter space. The next panel, i.e., Fig. 12b, therefore considers the case $y^L_{d\nu_e} = 0$. The region that results in a worse fit to IceCube data gets reduced compared to the non-zero $y^L_{d\nu_e}$ case as expected. Finally we show in Fig. 12c the allowed parameter space as a function of m_{S_1} considering $y^L_{d\nu_e} = y^L_{d\nu_\tau}$, with $y^L_{d\nu_\mu} = 0$. We see that for all the discussed cases, the IceCube results are comparable with LHC for masses below 1 TeV. However, in all three cases, the most stringent constraint comes from the low-energy flavor experiments denoted by pink points. The LHC direct searches from the LQ pair production currently exclude $m_{S_1} < 700 \text{ GeV}$ irrespective of the choice of couplings as long as LQ promptly decays. The single production of LQ at 8 TeV LHC [56] is also considered and we find that $y^L_{d\nu_e}$ as a function of m_{S_1} is more strongly constrained by the APV measurement than by the aforementioned analysis of the LHC data. This is similar to what has been discussed in Ref. [60].

The IceCube allowed parameter space in case of S_1 may change with the change in observed events in the future. The S_1 parameter space could be even more constrained if the current distribution of events persists in the future data, i.e., less events compared to SM + atmospheric prediction between the 300 TeV and 1000 TeV bins and more events in bins $> 1000 \text{ TeV}$. However, if the future data show the number of events in all the bins to be greater than the SM + atmospheric prediction, the S_1 LQ might become better suited scenario in explaining the PeV events.

The combined analysis of the constraints imposed by the LHC results, the IceCube data, and the low-energy flavor experiments on the U_1 parameter space can be summarized in Fig. 13. The green-shaded region is the one which results in a better or comparable fit with respect to the SM case. The brown bounded region just below green and in the lower part of Fig. 13 shows the parameter space which results in a fit worse than the SM at the level of 1%. The pink region in Fig. 13 is the one allowed by the flavor observables, radiative decays of the lepton as discussed in Sec. 5. The LHC constraints from the LQ pair production, in the dijet + MET, $j\bar{j}ee$, and $j\bar{j}\mu\mu$ final states are considered and the currently allowed space is shown by the gray meshed region. The region below 1.6 TeV is completely excluded by the LHC data for the choice of couplings considered here. The white region in Fig. 13 is excluded by all three sets of experimental constraints. The area within the purple boundary in the upper right side of Fig. 13 is allowed by both LHC and IceCube, taking into account the region resulting in a fit worse than the SM at the level of 1%. It can be seen from Figs. 9 and 13 that the region currently allowed by the low-energy observables results in a fit worse than the SM for the current IceCube data. Taking into account the parameter space resulting in a fit worse than SM at the level of 1%, the blue bounded region in the lower right side of Fig. 13, i.e., $m_{U_1} \geq 1.6 \text{ TeV}$ and $\chi^L_{de} < 0.05$, is currently

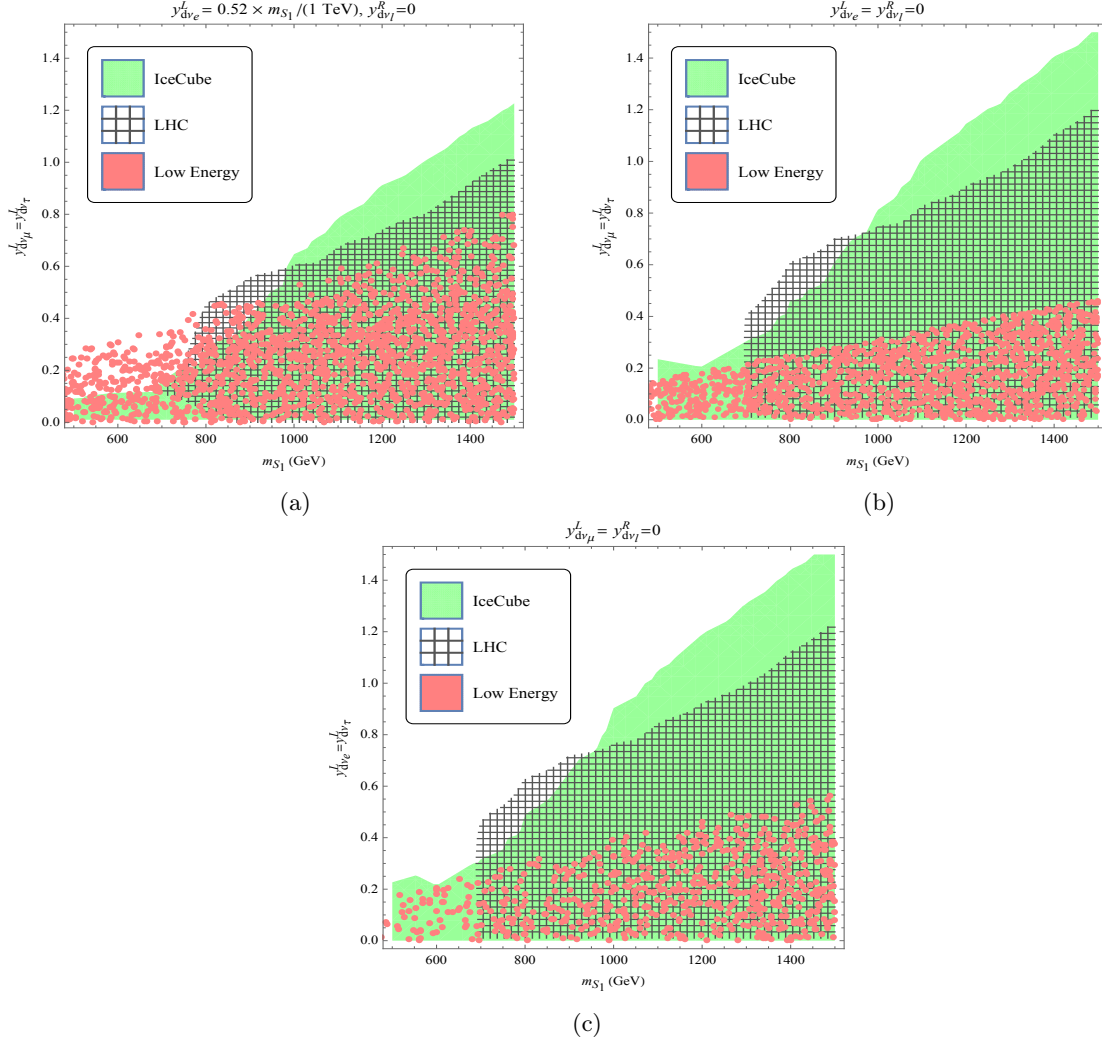


Figure 12: The currently allowed parameter space in the $m_{S_1} - (y_{d\nu_\ell}^L = y_{d\nu_{\ell'}}^L)$ plane, with $\ell \neq \ell'$ and $\ell, \ell' = e, \mu, \tau$. The green region gives a comparable fit to the SM prediction of the IceCube data up to the 1% disagreement level, grey-meshed region is from the LHC data. The pink points are allowed by the low-energy constraints discussed in Sec. 5.

allowed by all the experimental constraints considered in our work. Fig. 14 shows the corresponding analysis of the available parameter space for S_1 . The region denoted by a blue boundary still survives the LHC and the low-energy constraints and yields the fit of the IceCube data that is 1% or less away from the SM case.

We next discuss the effect of the couplings $y_{d\nu_\ell}^R$ on our results. The leading processes for LQ pair production at the LHC will be with the initial state of gg , $u\bar{u}$, and $d\bar{d}$. At large values of the right-handed $y_{d\nu_\ell}^R$ couplings the cross section in case of S_1 will be enhanced through the $d\bar{d}$ initial state. A large value of these couplings will also lead to a large branching ratio to $j\nu$ and is therefore strongly constrained by the search for the $jj\nu\nu$ final state at the LHC. We show in Fig. 15 the allowed parameter space from the LHC in red in the $y_{d\nu_e}^L - y_{d\nu_\ell}^R$ plane with the coupling $y_{d\nu_\mu}^L = y_{d\nu_\tau}^L = 0$ for $m_{S_1} = 800$ GeV (left panel) and 1 TeV (right panel). Since the IceCube data are more sensitive to the ν_e coupling we consider this particular choice to check the effect of $y_{d\nu_\ell}^R$ on $y_{d\nu_e}^L$. The contours in the plot show δ — the percent change in χ^2 from the SM value — as defined in Eq. (4.5). The result is almost independent of $y_{d\nu_\ell}^R$ for a particular value of $y_{d\nu_e}^L$. This is mainly because in the νN cross section the coupling $y_{d\nu_\ell}^R$ only appears quadratically in the final state. Apart from direct LHC searches $y_{d\nu_\ell}^R$ is also tightly constrained from the flavor observables, the allowed region shown by dotted points in Fig. 15. The inclusion of the U_1 couplings to the right-handed neutrinos follows the same pattern as in the S_1 case. Provided that the right-handed neutrinos do not contribute to the initial state, the current IceCube data is not sensitive to these couplings. The consideration of the right-handed neutrinos in the initial state will lead to a change in the initial flux at the source. This flux will depend on the mass of ν_ℓ^R and also on the possible decay channels in case of heavy ν_ℓ^R . This is beyond the scope of present analysis. The resulting final

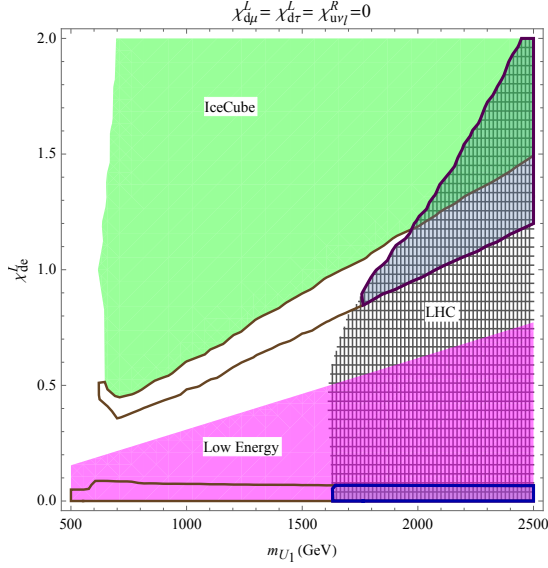


Figure 13: The allowed parameter space in $m_{U_1} - \chi_{de}^L$ region, with $\chi_{d\mu}^L = \chi_{d\tau}^L = 0$. The green-shaded region compared to the SM results in a better or comparable fit to the IceCube data, meshed region is allowed by LHC and the pink shaded region is the one allowed by the low-energy constraints discussed in Sec. 5. The white region is currently excluded by all the experiments.

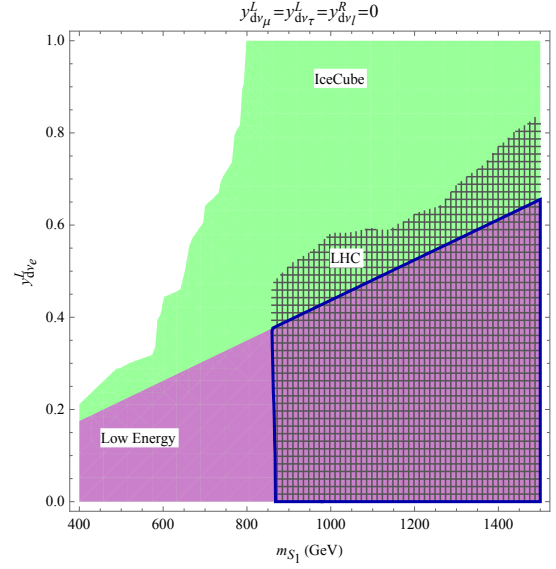


Figure 14: The allowed parameter space in $m_{S_1} - y_{de}^L$ region, with $y_{d\nu\mu}^L = y_{d\nu\tau}^L = 0$. The green-shaded region results in a worse fit of the IceCube data compared to SM at 1% level, meshed region is allowed by LHC and the pink shaded region is the one allowed by the low-energy constraints discussed in Sec. 5. The white region is currently excluded by all the experiments.

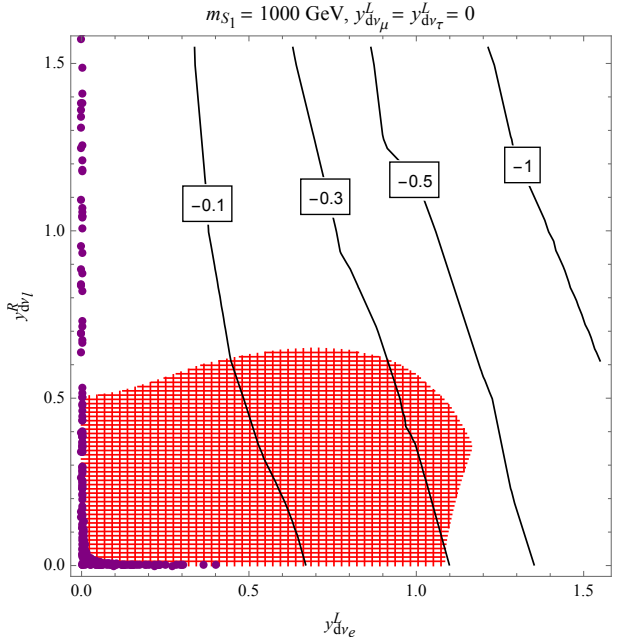
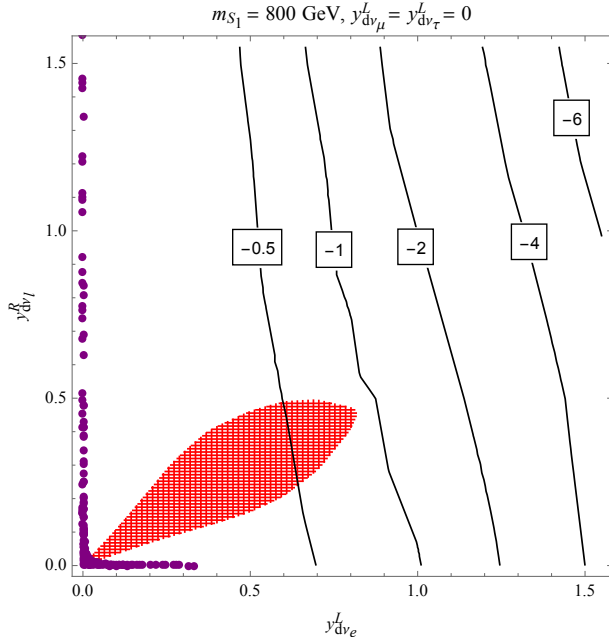


Figure 15: The allowed parameter space from LHC shown in red in the $y_{d\nu e}^L - y_{d\nu\ell}^R$ plane, with $y_{d\nu\mu}^L = y_{d\nu\tau}^L = 0$ for $m_{S_1} = 800$ GeV (left panel) and $m_{S_1} = 1$ TeV (right panel). The contours show the percent change in χ^2 as expressed by δ of Eq. (4.5). The dark pink points are allowed by the low-energy constraints discussed in Sec. 5.

high-energy cosmic neutrino flux ratios on earth by the possible mixing between the three active neutrinos and the fourth sterile neutrino have been studied in Ref. [61]. The explanation of the PeV neutrinos at IceCube, with the consideration of heavy right-handed neutrino, acting as a dark matter has been studied in Ref. [62].

Finally we show in the left (right) plot of Fig. 16 the contribution of U_1 (S_1) for mass of 900 GeV and $\chi_{de}^L = 2$ ($y_{d\nu e}^L = 2$), which gives $\delta = 16\%$ ($\delta = -4\%$). All the other couplings are set to zero. Note that

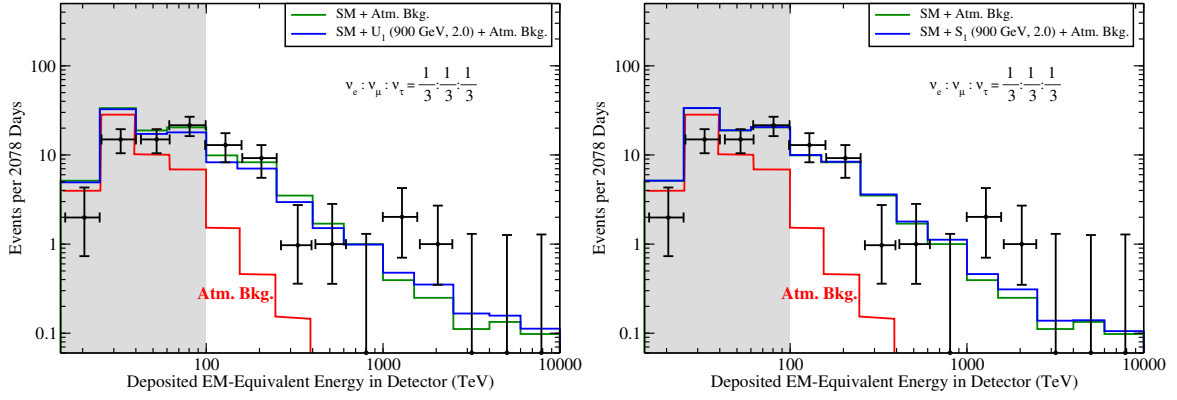


Figure 16: The total event rate, with the LQ contribution for $m_{U_1} = 900$ GeV ($\chi_{de}^L = 2$, $\chi_{d\mu}^L, \chi_{d\tau}^L = 0$) (left panel), and $m_{S_1} = 900$ GeV ($y_{d\nu_e}^L = 2$, $y_{d\nu_\mu}^L = y_{d\nu_\tau}^L = 0$) (right panel). The grey shaded region and the bin with zero events is not included in the fit.

even though the IceCube data alone favors U_1 over S_1 the actual parameter space allowed by the LHC and low-energy experiments of both U_1 and S_1 fits the IceCube data with the same level of disagreement.

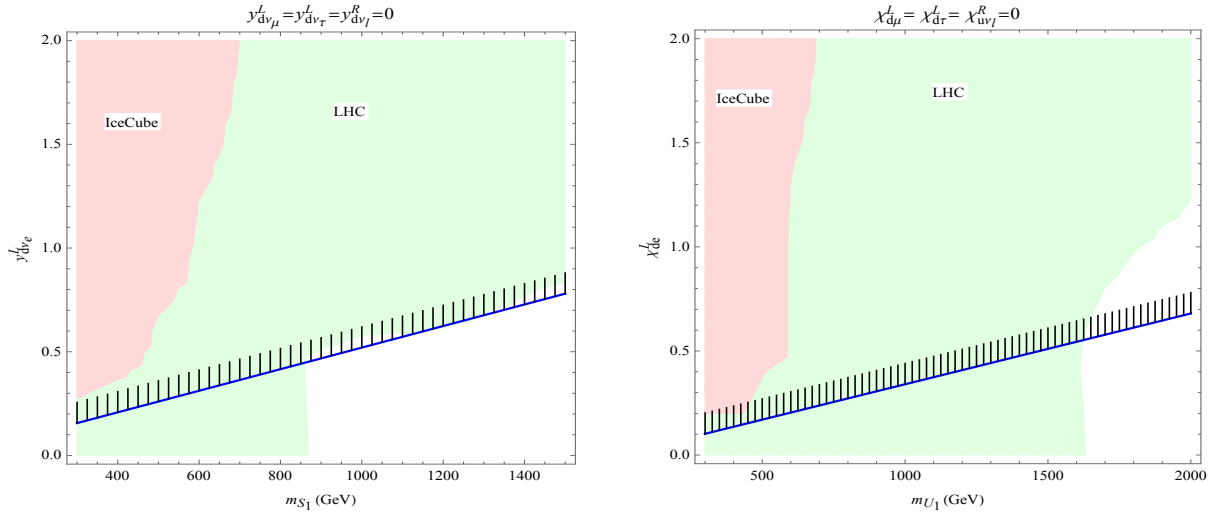


Figure 17: The $m_{S_1}-y_{d\nu_e}^L$ (left panel) and $m_{U_1}-\chi_{de}^L$ (right panel) parameter space where the shaded region shown in red is disallowed at 95% C.L. by the IceCube data. The region above the blue line is disallowed by APV. The green + red region is currently disallowed by the LHC data for the $jj\nu\nu$, $jj\mu\mu$, and $jj\mu\mu$ final states. The single LQ production is also included in the S_1 case. The white region below the blue line is currently allowed by all the experiments.

Our whole analysis has been done for the bins with non-zero events. We next present our results considering also the bins with zero events, where we split the events sample in 10 logarithmic energy bins each for showers and tracks. The neutrino in the 100 TeV–10 PeV energy range is considered with 20 logarithmic bins. We show in Fig. 17 the 95% C.L. allowed region in the $m_{S_1}-y_{d\nu_e}^L$ ($m_{U_1}-\chi_{de}^L$) parameter space for S_1 (U_1). The region in red is currently disallowed by IceCube at 95% C.L.. For our statistical analysis, the LQ mass and the couplings are kept as free parameters, with γ and C_0 fixed to the IceCube best fit data. The single LQ production is also considered in case of S_1 and is on par with the constraint from APV. The most stringent constraint currently comes from APV, with the white region below the blue line currently allowed by all the three experiments. We have used for our calculation the $(1/3 : 1/3 : 1/3)$ flavor ratio for the incoming flux, compatible with the current IceCube data. Overall we find that the 95% C.L. limits obtained from the IceCube data, considering zero event bins, are considerably weaker compared to the LQ direct searches at the 13 TeV LHC and the low-energy observables. This is mostly due to the current lack of statistics in the high-energy bins of the IceCube spectrum.

7 Conclusion

We analyse the constraints on the parameter space of the electroweak $SU(2)$ singlet scalar (vector) LQ S_1 (U_1) from IceCube and juxtapose them with the low-energy flavor and collider limits. In our set-up the leading NP contribution towards the neutrino-nucleon cross section in the S_1 (U_1) case is generated via S_1 -neutrino-down quark (U_1 -neutrino-up quark) interactions. The couplings of S_1 (U_1) to the up-type quarks and the charged leptons (neutrinos) are uniquely related to these interactions through the $SU(2)$ symmetry of the SM.

We find that S_1 worsens the SM fit of the IceCube data for the non-zero event bins when the deposited energy is in the 100 TeV–10 PeV range. The S_1 contribution always increases the SM one and accordingly the SM + S_1 scenario yields an enhanced number of events in each bin when compared to the SM case. This is beneficial for (detrimental to) the bins where there is an observed excess (lack) of events compared to the SM case especially since the SM agrees relatively well with the data. We accordingly constrain available parameter space for the S_1 mass and its couplings by requiring that a disagreement between the SM and the SM + S_1 fits of the current IceCube data is at most at the 1% level. The comparison of this parameter space with the constraints obtained by the 13 TeV LHC run and the low-energy flavor observables exhibits an overlapping region where the LQ mass is large and S_1 -neutrino-down quark coupling is small. The majority of the parameter space in the case of S_1 is ruled out by the low-energy flavor experiments.

On the other hand, U_1 exhibits an interference with the SM and can, in principle, improve the fit compared to the SM case by almost 16%. However, the parameter space associated with the best fit, i.e., $m_{U_1} = 900$ GeV and $\chi_{de}^L = 2.0$, is ruled out by both the LHC direct searches and the low-energy flavor experiments. In fact, the entire region in the m_{U_1} – χ_{de}^L plane that yields a better fit to the IceCube data compared to the SM case is in tension with the low-energy experiments. The region that is compatible with the low-energy and LHC data results, similarly to the S_1 case, in the IceCube fit that is 1% away from the SM case. This region corresponds to very small U_1 -neutrino-up quark coupling with $m_{U_1} \geq 1.6$ TeV. We have also verified that the couplings of both S_1 and U_1 to the right-handed neutrinos are not being sensitive to the current IceCube data provided that the right-handed neutrinos only contribute to the final state.

Acknowledgments We are grateful to Olcyr Sumensari, Boris Panes, and Damir Bečirević for helpful discussions. M.P. would like to thank Anushree Ghosh for discussions on IceCube. S.F. and M.P. acknowledge support of the Slovenian Research Agency through research core funding No. P1-0035.

A Formulas

We list here the different branching ratios used for our analysis in Sec. 5.

$$\text{BR}(D^0 \rightarrow \mu^+ \mu^-) = \tau_D f_D^2 m_D^3 \frac{G_F^2}{64\pi} \sqrt{1 - \frac{4m_\mu^2}{m_D^2}} \left| \frac{m_\mu}{m_D} \frac{v^2}{m_{S_1}^2} (V^* y^L)_{12} (V^* y^L)_{22} \right|^2 \quad (\text{A.1})$$

The $\pi \rightarrow \ell \bar{\nu}$ and the $\tau^- \rightarrow \pi^- \nu$ branching ratios at the leading order in SM are given by:

$$\begin{aligned} \text{BR}(\pi \rightarrow \ell \bar{\nu})|_{\text{SM}} &= \tau_\pi \frac{G_F^2}{8\pi} f_\pi^2 m_\pi m_\ell^2 |V_{11}|^2 \left(1 - \frac{m_\ell^2}{m_\pi^2}\right)^2, \\ \text{BR}(\tau^- \rightarrow \pi^- \nu)|_{\text{SM}} &= \tau_\tau \frac{G_F^2}{16\pi} f_\pi^2 m_\tau^3 |V_{11}|^2 \left(1 - \frac{m_\pi^2}{m_\tau^2}\right)^2. \end{aligned} \quad (\text{A.2})$$

The electroweak corrections to $\text{BR}(\pi \rightarrow \ell \bar{\nu})$ were calculated in Ref. [53] and for $\text{BR}(\tau^- \rightarrow \pi^- \nu)$ in Ref. [63]. The relevant branching ratios in the LQ models is given by,

$$\begin{aligned} \text{BR}(\pi \rightarrow \ell \bar{\nu}) &= \tau_\pi \frac{G_F^2}{8\pi} f_\pi^2 m_\pi^3 \left(1 - \frac{m_\ell^2}{m_\pi^2}\right)^2 \left[\frac{m_\ell^2}{m_\pi^2} |V_{11}|^2 + \frac{m_\ell^2}{m_\pi^2} \frac{2v^2}{C m_{\text{LQ}}^2} \text{Re} \left(V_{11}^* (y_{q\ell}^L)_{1j} \sum_{i=1}^3 U_{ji}^* (y_{q\nu}^L)_{1i} \right) \right. \\ &\quad \left. + \frac{v^2}{C m_{\text{LQ}}^2} \left(\frac{m_\ell}{m_\pi} (y_{q\ell}^L)_{1j} \sum_{i=1}^3 |(y_{q\nu}^L)_{1i}|^2 + C' \sum_{i=1}^3 |y_{1i}^R|^2 m_\pi^2 \left| \frac{(y_{q\ell}^L)_{1j}}{m_u + m_d} \right|^2 \right) \right], \\ \text{BR}(\tau^- \rightarrow \pi^- \nu) &= \tau_\tau \frac{G_F^2}{16\pi} f_\pi^2 m_\tau^2 m_\tau \left(1 - \frac{m_\pi^2}{m_\tau^2}\right)^2 \left[\frac{m_\tau^2}{m_\pi^2} |V_{11}|^2 + \frac{m_\tau^2}{m_\pi^2} \frac{v^2}{C m_{\text{LQ}}^2} \text{Re} \left(V_{11}^* (y_{q\ell}^L)_{13} \sum_{i=1}^3 U_{3i}^* (y_{q\nu}^L)_{1i} \right) \right] \end{aligned}$$

$$+ \frac{v^2}{C m_{LQ}^2} \left(\frac{m_\tau}{m_\pi} (y_{q\ell}^L)_{13} \sum_{i=1}^3 |(y_{q\nu}^L)_{1i}|^2 + C' \sum_{i=1}^3 |y_{1i}^R|^2 m_\pi^2 \left| \frac{(y_{q\ell}^L)_{13}}{m_u + m_d} \right|^2 \right) \Bigg], \quad (\text{A.3})$$

with $y_{q\nu}^L = y^L U(V^\dagger \chi^L U)$, $y_{q\ell}^L = V^* y^L (\chi^L)$, $C = 4(2)$, and $C' = 1(2)$ in the $S_1(U_1)$ case. The light quark masses are determined at the LQ mass scale. The subscript j in Eq. (A.3) takes on the values of 1 and 2 for e^- and μ^- respectively. The parameters relevant for the D meson, pion and the τ lepton properties are listed in Table 1.

τ_D (sec)	4.1×10^{-13}	τ_π	2.603×10^{-8}	τ_τ	2.903×10^{-13}
m_D (GeV)	1.86	m_π	0.140	m_τ	1.7768
m_c (GeV)	1.28	m_e	0.51×10^{-3}	m_μ	0.105
f_D (MeV)	212	f_π	130.41		

Table 1: Numerical values of parameters used in our calculation, taken from PDG [54].

References

- [1] M. G. Aartsen *et al.* [IceCube Collaboration], “Evidence for High-Energy Extraterrestrial Neutrinos at the IceCube Detector,” *Science* **342**, 1242856 (2013) [arXiv:1311.5238 [astro-ph.HE]].
- [2] M. G. Aartsen *et al.* [IceCube Collaboration], “Observation of High-Energy Astrophysical Neutrinos in Three Years of IceCube Data,” *Phys. Rev. Lett.* **113**, 101101 (2014) [arXiv:1405.5303 [astro-ph.HE]].
- [3] M. G. Aartsen *et al.* [IceCube Collaboration], “The IceCube Neutrino Observatory - Contributions to ICRC 2017 Part II: Properties of the Atmospheric and Astrophysical Neutrino Flux,” arXiv:1710.01191 [astro-ph.HE].
- [4] M. G. Aartsen *et al.* [IceCube Collaboration], “Neutrino emission from the direction of the blazar TXS 0506+056 prior to the IceCube-170922A alert,” *Science* **361**, no. 6398, 147 (2018) [arXiv:1807.08794 [astro-ph.HE]].
- [5] M. G. Aartsen *et al.* [IceCube and Fermi-LAT and MAGIC and AGILE and ASAS-SN and HAWC and H.E.S.S. and INTEGRAL and Kanata and Kiso and Kapteyn and Liverpool Telescope and Subaru and Swift NuSTAR and VERITAS and VLA/17B-403 Collaborations], “Multimessenger observations of a flaring blazar coincident with high-energy neutrino IceCube-170922A,” *Science* **361**, no. 6398, eaat1378 (2018) [arXiv:1807.08816 [astro-ph.HE]].
- [6] M. G. Aartsen *et al.* [IceCube Collaboration], “Search for steady point-like sources in the astrophysical muon neutrino flux with 8 years of IceCube data,” arXiv:1811.07979 [hep-ph].
- [7] H. Georgi and S. L. Glashow, “Unity of All Elementary Particle Forces,” *Phys. Rev. Lett.* **32**, 438 (1974).
- [8] S. S. Gershtein, A. A. Likhoded and A. I. Onishchenko, “TeV-scale leptoquarks from GUTs/string/M-theory unification,” *Phys. Rept.* **320**, 159 (1999).
- [9] R. Barbier *et al.*, “R-parity violating supersymmetry,” *Phys. Rept.* **420**, 1 (2005) [hep-ph/0406039].
- [10] B. Schrempp and F. Schrempp, “Light Leptoquarks,” *Phys. Lett.* **153B**, 101 (1985).
- [11] J. Wudka, “Composite Leptoquarks,” *Phys. Lett.* **167B**, 337 (1986).
- [12] I. Doršner, S. Fajfer, A. Greljo, J. F. Kamenik and N. Košnik, “Physics of leptoquarks in precision experiments and at particle colliders,” *Phys. Rept.* **641**, 1 (2016) [arXiv:1603.04993 [hep-ph]].
- [13] R. Aaij *et al.* [LHCb Collaboration], “Test of lepton universality using $B^+ \rightarrow K^+ \ell^+ \ell^-$ decays,” *Phys. Rev. Lett.* **113**, 151601 (2014) [arXiv:1406.6482 [hep-ex]].
- [14] R. Aaij *et al.* [LHCb Collaboration], “Measurement of the ratio of branching fractions $\mathcal{B}(\bar{B}^0 \rightarrow D^{*+} \tau^- \bar{\nu}_\tau) / \mathcal{B}(\bar{B}^0 \rightarrow D^{*+} \mu^- \bar{\nu}_\mu)$,” *Phys. Rev. Lett.* **115**, no. 11, 111803 (2015) Erratum: [*Phys. Rev. Lett.* **115**, no. 15, 159901 (2015)] [arXiv:1506.08614 [hep-ex]].

- [15] R. Aaij *et al.* [LHCb Collaboration], “Test of lepton universality with $B^0 \rightarrow K^{*0} \ell^+ \ell^-$ decays,” JHEP **1708**, 055 (2017) [arXiv:1705.05802 [hep-ex]].
- [16] M. Bauer and M. Neubert, “Minimal Leptoquark Explanation for the $R_{D^{(*)}}$, R_K , and $(g-2)_g$ Anomalies,” Phys. Rev. Lett. **116**, no. 14, 141802 (2016) [arXiv:1511.01900 [hep-ph]].
- [17] D. Bečirević, S. Fajfer, N. Košnik and O. Sumensari, “Leptoquark model to explain the B -physics anomalies, R_K and R_D ,” Phys. Rev. D **94**, no. 11, 115021 (2016) [arXiv:1608.08501 [hep-ph]].
- [18] A. Crivellin, D. Müller and T. Ota, “Simultaneous explanation of $R(D^{(*)})$ and $b \rightarrow s \mu^+ \mu^-$: the last scalar leptoquarks standing,” JHEP **1709**, 040 (2017) [arXiv:1703.09226 [hep-ph]].
- [19] D. Buttazzo, A. Greljo, G. Isidori and D. Marzocca, “B-physics anomalies: a guide to combined explanations,” JHEP **1711**, 044 (2017) [arXiv:1706.07808 [hep-ph]].
- [20] A. Crivellin and F. Saturnino, “Correlating Tauonic B Decays to the Neutron EDM via a Scalar Leptoquark,” arXiv:1905.08257 [hep-ph].
- [21] L. Di Luzio, A. Greljo and M. Nardecchia, “Gauge leptoquark as the origin of B-physics anomalies,” Phys. Rev. D **96**, no. 11, 115011 (2017) [arXiv:1708.08450 [hep-ph]].
- [22] L. Calibbi, A. Crivellin and T. Li, “Model of vector leptoquarks in view of the B -physics anomalies,” Phys. Rev. D **98**, no. 11, 115002 (2018) [arXiv:1709.00692 [hep-ph]].
- [23] M. Bordone, C. Cornella, J. Fuentes-Martin and G. Isidori, “A three-site gauge model for flavor hierarchies and flavor anomalies,” Phys. Lett. B **779**, 317 (2018) [arXiv:1712.01368 [hep-ph]].
- [24] C. Cornella, J. Fuentes-Martin and G. Isidori, “Revisiting the vector leptoquark explanation of the B-physics anomalies,” arXiv:1903.11517 [hep-ph].
- [25] P. Abreu *et al.* [DELPHI Collaboration], “Limits on the production of scalar leptoquarks from Z0 decays at LEP,” Phys. Lett. B **316**, 620 (1993).
- [26] S. Aid *et al.* [H1 Collaboration], “A Search for leptoquarks at HERA,” Phys. Lett. B **369**, 173 (1996) [hep-ex/9512001].
- [27] H. Abramowicz *et al.* [ZEUS Collaboration], “Search for first-generation leptoquarks at HERA,” Phys. Rev. D **86**, 012005 (2012) [arXiv:1205.5179 [hep-ex]].
- [28] C. Grosso-Pilcher *et al.* [CDF and D0 Collaborations], “Combined limits on first generation leptoquarks from the CDF and D0 experiments,” hep-ex/9810015.
- [29] V. M. Abazov *et al.* [D0 Collaboration], “Search for pair production of second generation scalar leptoquarks,” Phys. Lett. B **671**, 224 (2009) [arXiv:0808.4023 [hep-ex]].
- [30] M. Aaboud *et al.* [ATLAS Collaboration], “Search for scalar leptoquarks in pp collisions at $\sqrt{s}=13$ TeV with the ATLAS experiment,” New J. Phys. **18**, no. 9, 093016 (2016) [arXiv:1605.06035 [hep-ex]].
- [31] CMS Collaboration [CMS Collaboration], “Search for pair-production of first generation scalar leptoquarks in pp collisions at $\sqrt{s} = 13$ TeV with 2.6 fb $^{-1}$,” CMS-PAS-EXO-16-043.
- [32] CMS Collaboration [CMS Collaboration], “Search for pair-production of second-generation scalar leptoquarks in pp collisions at $\sqrt{s} = 13$ TeV with the CMS detector,” CMS-PAS-EXO-16-007.
- [33] M. Schmaltz and Y. M. Zhong, “The leptoquark Hunter’s guide: large coupling,” JHEP **1901**, 132 (2019) [arXiv:1810.10017 [hep-ph]].
- [34] P. Bandyopadhyay and R. Mandal, “Revisiting scalar leptoquark at the LHC,” Eur. Phys. J. C **78**, 491 (2018) [arXiv:1801.04253 [hep-ph]].
- [35] U. K. Dey, D. Kar, M. Mitra, M. Spannowsky and A. C. Vincent, “Searching for Leptoquarks at IceCube and the LHC,” Phys. Rev. D **98**, no. 3, 035014 (2018) [arXiv:1709.02009 [hep-ph]].
- [36] N. Mileo, A. de la Puente and A. Szykman, “Implications of a Electroweak Triplet Scalar Leptoquark on the Ultra-High Energy Neutrino Events at IceCube,” JHEP **1611**, 124 (2016) [arXiv:1608.02529 [hep-ph]].

- [37] B. Chauhan, B. Kindra and A. Narang, “Discrepancies in simultaneous explanation of flavor anomalies and IceCube PeV events using leptoquarks,” *Phys. Rev. D* **97**, no. 9, 095007 (2018) [arXiv:1706.04598 [hep-ph]].
- [38] V. Barger and W. Y. Keung, “Superheavy Particle Origin of IceCube PeV Neutrino Events,” *Phys. Lett. B* **727**, 190 (2013) [arXiv:1305.6907 [hep-ph]].
- [39] B. Dutta, Y. Gao, T. Li, C. Rott and L. E. Strigari, “Leptoquark implication from the CMS and IceCube experiments,” *Phys. Rev. D* **91**, 125015 (2015) [arXiv:1505.00028 [hep-ph]].
- [40] U. K. Dey and S. Mohanty, “Constraints on Leptoquark Models from IceCube Data,” *JHEP* **1604**, 187 (2016) [arXiv:1505.01037 [hep-ph]].
- [41] D. Bečirević, B. Panes, O. Sumensari and R. Zukanovich Funchal, “Seeking leptoquarks in IceCube,” *JHEP* **1806**, 032 (2018) [arXiv:1803.10112 [hep-ph]].
- [42] L. A. Anchordoqui, C. A. Garcia Canal, H. Goldberg, D. Gomez Dumm and F. Halzen, “Probing leptoquark production at IceCube,” *Phys. Rev. D* **74**, 125021 (2006) [hep-ph/0609214].
- [43] P. S. B. Dev, D. K. Ghosh and W. Rodejohann, “R-parity Violating Supersymmetry at IceCube,” *Phys. Lett. B* **762**, 116 (2016) [arXiv:1605.09743 [hep-ph]].
- [44] A. D. Martin, W. J. Stirling, R. S. Thorne and G. Watt, “Parton distributions for the LHC,” *Eur. Phys. J. C* **63**, 189 (2009) [arXiv:0901.0002 [hep-ph]].
- [45] R. Gandhi, C. Quigg, M. H. Reno and I. Sarcevic, “Ultrahigh-energy neutrino interactions,” *Astropart. Phys.* **5**, 81 (1996) [hep-ph/9512364].
- [46] M. G. Aartsen *et al.* [IceCube Collaboration], “Flavor Ratio of Astrophysical Neutrinos above 35 TeV in IceCube,” *Phys. Rev. Lett.* **114**, no. 17, 171102 (2015) [arXiv:1502.03376 [astro-ph.HE]].
- [47] M. G. Aartsen *et al.* [IceCube Collaboration], “Measurements using the inelasticity distribution of multi-TeV neutrino interactions in IceCube,” *Phys. Rev. D* **99**, no. 3, 032004 (2019) [arXiv:1808.07629 [hep-ex]].
- [48] S. Palomares-Ruiz, A. C. Vincent and O. Mena, “Spectral analysis of the high-energy IceCube neutrinos,” *Phys. Rev. D* **91**, no. 10, 103008 (2015) [arXiv:1502.02649 [astro-ph.HE]].
- [49] A. M. Baldini *et al.* [MEG Collaboration], “Search for the lepton flavour violating decay $\mu^+ \rightarrow e^+ \gamma$ with the full dataset of the MEG experiment,” *Eur. Phys. J. C* **76**, no. 8, 434 (2016) [arXiv:1605.05081 [hep-ex]].
- [50] B. Aubert *et al.* [BaBar Collaboration], “Searches for Lepton Flavor Violation in the Decays $\tau^\pm \rightarrow e^\pm \gamma$ and $\tau^\pm \rightarrow \mu^\pm \gamma$,” *Phys. Rev. Lett.* **104**, 021802 (2010) [arXiv:0908.2381 [hep-ex]].
- [51] R. Aaij *et al.* [LHCb Collaboration], “Search for the rare decay $D^0 \rightarrow \mu^+ \mu^-$,” *Phys. Lett. B* **725**, 15 (2013) [arXiv:1305.5059 [hep-ex]].
- [52] S. Fajfer and N. Košnik, “Prospects of discovering new physics in rare charm decays,” *Eur. Phys. J. C* **75**, no. 12, 567 (2015). [arXiv:1510.00965 [hep-ph]].
- [53] V. Cirigliano and I. Rosell, “Two-loop effective theory analysis of $\pi(K) \rightarrow e \text{ anti-}\nu_e/\gamma$ branching ratios,” *Phys. Rev. Lett.* **99**, 231801 (2007) [arXiv:0707.3439 [hep-ph]].
- [54] M. Tanabashi *et al.* [Particle Data Group], “Review of Particle Physics,” *Phys. Rev. D* **98**, no. 3, 030001 (2018).
- [55] P. Arnan, D. Bečirević, F. Mescia and O. Sumensari, “Probing low energy scalar leptoquarks by the leptonic W and Z couplings,” *JHEP* **1902**, 109 (2019) [arXiv:1901.06315 [hep-ph]].
- [56] V. Khachatryan *et al.* [CMS Collaboration], “Search for single production of scalar leptoquarks in proton-proton collisions at $\sqrt{s} = 8$ TeV,” *Phys. Rev. D* **93**, no. 3, 032005 (2016) Erratum: [*Phys. Rev. D* **95**, no. 3, 039906 (2017)] [arXiv:1509.03750 [hep-ex]].
- [57] S. Bansal, R. M. Capdevilla, A. Delgado, C. Kolda, A. Martin and N. Raj, “Hunting leptoquarks in monolepton searches,” *Phys. Rev. D* **98**, no. 1, 015037 (2018) [arXiv:1806.02370 [hep-ph]].

- [58] A. M. Sirunyan *et al.* [CMS Collaboration], “Constraints on models of scalar and vector leptoquarks decaying to a quark and a neutrino at $\sqrt{s} = 13$ TeV,” Phys. Rev. D **98**, no. 3, 032005 (2018) [arXiv:1805.10228 [hep-ex]].
- [59] CMS Collaboration [CMS Collaboration], “Constraints on models of scalar and vector leptoquarks decaying to a quark and a neutrino at $\sqrt{s} = 13$ TeV,” CMS-PAS-SUS-18-001.
- [60] N. Raj, “Anticipating nonresonant new physics in dilepton angular spectra at the LHC,” Phys. Rev. D **95**, no. 1, 015011 (2017) [arXiv:1610.03795 [hep-ph]].
- [61] H. Athar, M. Jezabek and O. Yasuda, “Effects of neutrino mixing on high-energy cosmic neutrino flux,” Phys. Rev. D **62**, 103007 (2000) [hep-ph/0005104].
- [62] P. S. B. Dev, D. Kazanas, R. N. Mohapatra, V. L. Teplitz and Y. Zhang, “Heavy right-handed neutrino dark matter and PeV neutrinos at IceCube,” JCAP **1608**, no. 08, 034 (2016) [arXiv:1606.04517 [hep-ph]].
- [63] J. Erler, “Electroweak radiative corrections to semileptonic tau decays,” Rev. Mex. Fis. **50**, 200 (2004) [hep-ph/0211345].